

Figure 3 Molecular analyses of the *PLP1* duplication identified in Patient 1. (a) The result of a custom-designed aCGH shows partial duplication of *PLP1*. (b) A schematic representation of the breakpoint analyzed by PCR and subsequent sequencing. (c) A 775 bp PCR product including a breakpoint is amplified by Primer A and B and is shown in electrophoresis. m; molecular marker OneSTEP Ladder 50 (Nippon Gene).

the previous study.¹² Finally, total RNA samples extracted from the 12 iPS cell clones generated in this study were analyzed. Although we could detect the *PLP1* band in iPS cells from normal individual and Patients 2 and 3, we could not detect the *PLP1* band in the iPS cells generated from Patient 1, indicating null expression of *PLP1* caused by the partial duplication of *PLP1* (Figure 5). In Patients 2 and 3, *PLP1* signals appeared to be somewhat stronger than in controls, but because of the large variation in signal intensity among different cell lines, it was inconclusive in our limited experiments.

DISCUSSION

In this study, we identified different *PLP1* abnormalities in three patients with PMD. Patient 3 showed a novel missense mutation, c.636G>C (Tyr212Cys), which is in the extramembrane region of the PLP1 protein.² A missense substitution in the same codon, but resulting in a change into a different amino acid, c.634T>C (Tyr212Arg), has been reported to be a pathogenetic mutation by others.¹³ Frequently, a cysteine residue changes the three-dimensional protein conformation drastically owing to disulfide bond formation

with other cysteines.¹⁴ Thus, the amino-acid substitution to cysteine in our patient is likely a pathogenetic mutation, causing PMD. Previous genotype-phenotype correlation study showed that the phenotype of patients with *PLP1* missense mutations was more severe than those with *PLP1* duplications.¹⁻³ Indeed, Patient 3 showed severely delayed psychomotor development complicated by respiratory and feeding difficulties. His condition can be classified as form 0 according to the classification proposed by Cailloux *et al.*,¹³ as form 0 is the most severe form of PMD. Dysmyelination in this patient was particularly severe.

Patient 2 had a 0.6-Mb duplication including *PLP1*. This size is typical for PMD patients with *PLP1* duplications.^{8,15,16} This patient is now 43 years old and does not show any deterioration of neurological abilities. Despite being bedridden, he can verbally communicate with several words. His clinical condition can be classified as form 2, because his maximum motor ability was sitting. His dysmyelination is milder than that of Patient 3.

The most intriguing result in this study is the partial duplication of *PLP1* identified in Patient 1. Although there have been reports

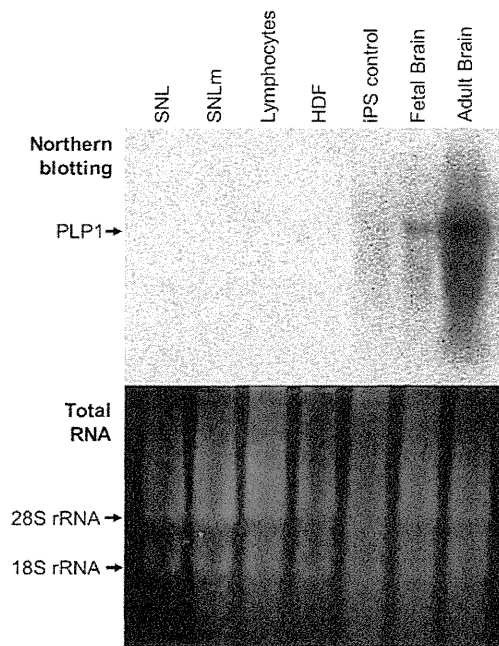


Figure 4 *PLP1* expression analysis by the northern blotting for various samples. (Upper) Predominant expression of *PLP1* is shown in the brain samples. Although control iPS cells show weak expression, there are no expressions of *PLP1* in the other samples. (Bottom) Agarose gel staining for the total RNAs before subsequent northern blotting indicates the same amounts of total RNAs loaded in each lane. SNLm, SNL-feeder cells treated with mitomycin; HDF, human dermal fibroblasts

of partial deletions in *PLP1* identified by multiplex ligation-dependent probe amplification analysis,⁹ this is the first report of a partial duplication of *PLP1*. The duplicated segment included the promoter region and the first three exons. Therefore, we hypothesized that a very short mRNA or long fusion mRNA might be expressed by this duplication together with the normal mRNA. To confirm this hypothesis, we analyzed *PLP1* expression by using northern blot analysis, the only way to detect the length and the quantity of mRNAs. As expression levels of *PLP1* in skin fibroblasts were too low to be examined by northern blot analysis, we generated iPS cells from the patients. Contrary to expectation, northern blot analysis showed no *PLP1* bands in the iPS cell generated from the fibroblasts of Patient 1. Although there may be a limitation to detect short-unstable mRNAs in our method, this possibly indicated that the expression of *PLP1* mRNA was disturbed by the *PLP1* partial duplication identified in Patient 1. Regarding the clinical severities of the patients, Patient 1 showed milder phenotype than Patient 2, and his condition can be classified as form 3. Previous genotype-phenotype correlation study have shown that patients with *PLP1* missense mutations show severe manifestation associated with severe hypomyelination, which is recognized as the consequence of accumulated mutant protein in the endoplasmic reticulum as a gain-of-toxic function of the mutant protein.² Excessive *PLP1* protein resulting from genomic duplications may accumulate in late endosomes/lysosomes, promoting its incorporation into other myelin components.⁴ In contrast, patients with *PLP1* null mutations escape severe impairments because of the absence of any gain-of-toxic function.^{2,13,17} Indeed, knockout mice with a functionally null *Plp1* gene do not develop classical signs of *Plp1*-related disease; their

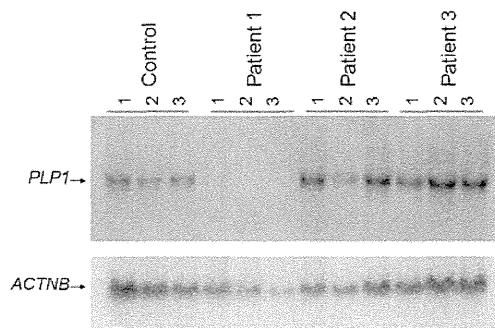


Figure 5 *PLP1* expression analyses using northern blotting. Three iPS cells of Patient 1 show no *PLP1* band, whereas the other iPS cells from normal control, Patient 2 and Patient 3 show expressions of *PLP1*. *ACTNB* (actin beta) is used for internal control.

oligodendrocytes develop normally and synthesize compact myelin sheaths.^{3,18} However, the mice show ultrastructural abnormalities, including swelling of the small-diameter axons and late-onset axonal degeneration.^{3,19} Consequently, a loss-of-function mutation of *PLP1* does not induce oligodendrocyte cell death, possibly serving as a mechanism underlying the milder phenotypic consequences observed in patients with null *PLP1* mutations. Although length-dependent axonal degeneration has been described in *PLP1* null mutations,²⁰ there is no information about peripheral neuropathy in Patient 1. Thus, it was unclear whether the clinical condition of Patient 1 is compatible with that of *PLP1* null mutations. However, the lack of *PLP1* expression in iPS cells derived from Patient 1 clearly demonstrated that the underlying mechanism of PMD in Patient 1, with a partial *PLP1* duplication, is different from the other two patients in this study.

Immortalized lymphocytes and skin fibroblasts derived from patients are often used for expression studies or biological analyses, as these cells are easy to be obtained and handled. However, many tissue-specific genes are not sufficiently expressed by these cells; *PLP1* being one of them. Although there are reports examining *PLP1* expression by RT-PCR, using mRNA extracted from skin fibroblasts,^{4,5,21} the expression of *PLP1* mRNA in skin fibroblasts is too low to be examined by northern blotting as shown here. In this study, our microarray database search showed over 40 times higher *PLP1* expression in iPS cells than that in skin fibroblasts. Our initial northern blot analysis confirmed faint but detectable *PLP1* expression in iPS cells, whereas no expression was observed in skin fibroblasts, lymphocytes or SNL feeder cells. This study also confirmed a lack of *PLP1* expression in SNL feeder cells. Therefore, this study demonstrates that iPS cells express endogenous *PLP1*, and that the possibility of contamination from SNL feeder cells or original skin fibroblasts can be excluded. Although being detectable by northern blotting, *PLP1* expression in iPS cells appeared to be much lower than that in mature oligodendrocytes and may be simply cryptic rather than functional. If so, this allows us to evaluate the native transcriptional level of each mutant (and wild-type) *PLP1* allele, which is the primary focus of our study. Meanwhile, terminal differentiation of iPS cells into the oligodendrocyte lineage would result in an enhanced *PLP1* expression with functional consequence. However, this requires technological breakthrough in the induction of terminal differentiation into oligodendrocyte lineage, which is currently unavailable.

In conclusion, we identified the first PMD patient having a partial *PLP1* duplication. The absence of *PLP1* expression in iPSC cells, generated from the patient's skin fibroblasts, proved the underlying effects of the partial *PLP1* duplication for the PMD development.

CONFLICT OF INTEREST

The authors declare no conflict of interest.

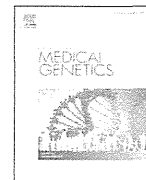
ACKNOWLEDGEMENTS

We thank the patients and their families for their cooperation. This work was mainly supported by JST PRESTO program (KS) and was partially supported by Grant-in-Aid for Scientific Research on Innovated Areas 'Foundation of Synapse and Neurocircuit Pathology' and Grant-in-Aid for scientific research from Health Labor Sciences Research Grants from the Ministry of Health, Labor and Welfare, Japan (TY). This work was supported in part by Grant-in-Aid for Scientific Research (A) 21249062, Japan Society for the Promotion of Science (JSPS) and 'High-Tech Research Center' Project for Private Universities: matching fund subsidy from the Ministry of Education, Culture, Sports, Science and Technology, 2006–2010 'The Research Center for the Molecular Pathomechanisms of Epilepsy, Fukuoka University', Research Grants (21B-5) for Nervous and Mental Disorder from the Ministry of Health, Labor and Welfare and Health and Labor Science Research Grant 21210301, KB220001 from the Ministry of Health, Labor and Welfare, and Adaptable and Seamless Technology Transfer Program through Target-driven R&D (A-STEP) Exploratory Research, Japan Science and Technology Agency (JSP) (SH). KS thanks Hayashi Memorial Foundation for Female Natural Scientists for grant aid support.

WEB SITE: NCBI GEO; <http://www.ncbi.nlm.nih.gov/guide/genes-expression/OMIM>; <http://omim.org>

- Inoue, K. PLP1-related inherited dysmyelinating disorders: Pelizaeus-Merzbacher disease and spastic paraplegia type 2. *Neurogenetics* **6**, 1–16 (2005).
- Garbern, J.Y. Pelizaeus-Merzbacher disease: Genetic and cellular pathogenesis. *Cell. Mol. Life Sci.* **64**, 50–65 (2007).
- Woodward, K.J. The molecular and cellular defects underlying Pelizaeus-Merzbacher disease. *Expert. Rev. Mol. Med.* **10**, e14 (2008).
- Hobson, G.M., Huang, Z., Sperle, K., Sistermans, E., Rogan, P.K., Garbern, J.Y. *et al.* Splice-site contribution in alternative splicing of PLP1 and DM20: molecular studies in oligodendrocytes. *Hum. Mutat.* **27**, 69–77 (2006).
- Regis, S., Grossi, S., Corsolini, F., Biancheri, R. & Filocamo, M. PLP1 gene duplication causes overexpression and alteration of the PLP/DM20 splicing balance in fibroblasts from Pelizaeus-Merzbacher disease patients. *Biochim. Biophys. Acta.* **1792**, 548–554 (2009).
- Inoue, H. Neurodegenerative disease-specific induced pluripotent stem cell research. *Exp. Cell. Res.* **316**, 2560–2564 (2010).
- Takahashi, K., Tanabe, K., Ohnuki, M., Narita, M., Ichisaka, T., Tomoda, K. *et al.* Induction of pluripotent stem cells from adult human fibroblasts by defined factors. *Cell* **131**, 861–872 (2007).
- Shimojima, K., Inoue, T., Hoshino, A., Kakiuchi, S., Watanabe, Y., Sasaki, M. *et al.* Comprehensive genetic analyses of PLP1 in patients with Pelizaeus-Merzbacher disease applied by array-CGH and fiber-FISH analyses identified new mutations and variable sizes of duplications. *Brain Dev.* **32**, 171–179 (2010).
- Warshawsky, I., Chernova, O.B., Hubner, C.A., Stindl, R., Henneke, M., Gal, A. *et al.* Multiplex ligation-dependent probe amplification for rapid detection of proteolipid protein 1 gene duplications and deletions in affected males and carrier females with Pelizaeus-Merzbacher disease. *Clin. Chem.* **52**, 1267–1275 (2006).
- Ohnuki, M., Takahashi, K. & Yamanaka, S. Generation and characterization of human induced pluripotent stem cells. *Curr. Protoc. Stem Cell Biol.* Chapter 4, Unit 4A2 (2009).
- Yamamoto, T., Feng, J.H., Higaki, K., Taniguchi, M., Nanba, E., Ninomiya, H. *et al.* Increased NPC1 mRNA in skin fibroblasts from Niemann-Pick disease type C patients. *Brain Dev.* **26**, 245–250 (2004).
- Iwaki, A., Muramoto, T., Iwaki, I., Furumi, H., Dario-deLeon, M.L., Tateishi, J. *et al.* A missense mutation in the proteolipid protein gene responsible for Pelizaeus-Merzbacher disease in a Japanese family. *Hum. Mol. Genet.* **2**, 19–22 (1993).
- Cailloux, F., Gauthier-Barichard, F., Mimault, C., Isabelle, V., Courtois, V., Giraud, G. *et al.* Genotype-phenotype correlation in inherited brain myelination defects due to proteolipid protein gene mutations. Clinical European Network on Brain Demyelinating Disease. *Eur. J. Hum. Genet.* **8**, 837–845 (2000).
- Dhaunchak, A.S. & Nave, K.A. A common mechanism of PLP/DM20 misfolding causes cysteine-mediated endoplasmic reticulum retention in oligodendrocytes and Pelizaeus-Merzbacher disease. *Proc. Natl Acad. Sci. USA* **104**, 17813–17818 (2007).
- Lee, J.A., Inoue, K., Cheung, S.W., Shaw, C.A., Stankiewicz, P. & Lupski, J.R. Role of genomic architecture in PLP1 duplication causing Pelizaeus-Merzbacher disease. *Hum. Mol. Genet.* **15**, 2250–2265 (2006).
- Woodward, K.J., Cundall, M., Sperle, K., Sistermans, E.A., Ross, M., Howell, G. *et al.* Heterogeneous duplications in patients with Pelizaeus-Merzbacher disease suggest a mechanism of coupled homologous and nonhomologous recombination. *Am. J. Hum. Genet.* **77**, 966–987 (2005).
- Sistermans, E.A., de Wijs, I.J., de Coo, R.F., Smit, L.M., Menko, F.H. & van Oost, B.A. A (G-to-A) mutation in the initiation codon of the proteolipid protein gene causing a relatively mild form of Pelizaeus-Merzbacher disease in a Dutch family. *Hum. Genet.* **97**, 337–339 (1996).
- Klugmann, M., Schwab, M.H., Puhlhofer, A., Schneider, A., Zimmermann, F., Griffiths, I.R. *et al.* Assembly of CNS myelin in the absence of proteolipid protein. *Neuron* **18**, 59–70 (1997).
- Griffiths, I., Klugmann, M., Anderson, T., Yool, D., Thomson, C., Schwab, M.H. *et al.* Axonal swellings and degeneration in mice lacking the major proteolipid of myelin. *Science* **280**, 1610–1613 (1998).
- Garbern, J.Y., Yool, D.A., Moore, G.J., Wilds, I.B., Faulk, M.W., Klugmann, M. *et al.* Patients lacking the major CNS myelin protein, proteolipid protein 1, develop length-dependent axonal degeneration in the absence of demyelination and inflammation. *Brain* **125**, 551–561 (2002).
- Mikesova, E., Barankova, L., Sakmaryova, I., Tatarikova, I. & Seeman, P. Quantitative multiplex real-time PCR for detection of PLP1 gene duplications in Pelizaeus-Merzbacher patients. *Genet. Test.* **10**, 215–220 (2006).

Supplementary Information accompanies the paper on Journal of Human Genetics website (<http://www.nature.com/jhg>)



Short clinical report

Pelizaeus-Merzbacher disease caused by a duplication-inverted triplication-duplication in chromosomal segments including the *PLP1* region

Keiko Shimojima^a, Toshiyuki Mano^b, Mitsuru Kashiwagi^c, Takuya Tanabe^d, Midori Sugawara^a, Nobuhiko Okamoto^e, Hiroshi Arai^f, Toshiyuki Yamamoto^{a,*}

^a Tokyo Women's Medical University Institute for Integrated Medical Sciences, Tokyo, Japan

^b Department of Pediatric Neurology, Osaka Medical Center and Research Institute for Maternal and Child Health, Osaka, Japan

^c Division of Pediatrics, Hirakata City Hospital, Hirakata, Japan

^d Department of Pediatric Neurology, Tanabe-Kadobayashi Children's Clinic, Hirakata, Japan

^e Department of Medical Genetics, Osaka Medical Center and Research Institute for Maternal and Child Health, Osaka, Japan

^f Department of Pediatric Neurology, Morinomiya Hospital, Osaka, Japan

ARTICLE INFO

Article history:

Received 28 September 2011

Accepted 29 February 2012

Available online 21 March 2012

Keywords:

Pelizaeus-Merzbacher disease (PMD)

Proteolipid protein 1 (*PLP1*)

Microarray-based comparative genomic hybridization (aCGH)

Fluorescence *in situ* hybridization (FISH)

Triplication

DUP-TRP/INV-DUP

ABSTRACT

Pelizaeus-Merzbacher disease (PMD; MIM#312080) is a rare X-linked leukodystrophy presenting with motor developmental delay associated with spasticity and nystagmus. PMD is mainly caused by abnormalities in the proteolipid protein 1 gene (*PLP1*), most frequently due to duplications of chromosomal segments including *PLP1*. In this study, a 9-year-old male patient manifesting severe developmental delay and spasticity was analyzed for *PLP1* alteration, and triplication of *PLP1* was identified. Further examination revealed an underlying genomic organization, duplication-inverted triplication-duplication (DUP-TRP/INV-DUP), in which a triplicated segment was nested between 2 junctions. One of the 2 junctions was caused by inverted homologous regions, and the other was caused by non-homologous end-joining. PMD patients with *PLP1* duplications usually show milder-classical forms of the disease compared with patients with *PLP1* missense mutations manifesting severe congenital forms. The present patient showed severe phenotypic features that represent an intermediate form of PMD between classical and congenital forms. This is the first report of a patient with *PLP1* triplication caused by a DUP-TRP/INV-DUP structure. This study adds additional evidence about the consequences of *PLP1* triplication.

© 2012 Elsevier Masson SAS. All rights reserved.

1. Introduction

Pelizaeus-Merzbacher disease (PMD; MIM#312080) is a rare X-linked leukodystrophy presenting with nystagmus, hypotonia that later develops into spasticity, dystonia, ataxia, and developmental delay beginning in the first year of life [4,9]. The proteolipid protein 1 gene (*PLP1*; MIM#300401) is the main responsible gene for PMD and the most common *PLP1* alterations are gene duplications, which are found in 60–70% of PMD patients [4,9]. Nucleotide alterations that affect the amino acid sequences of *PLP1* are found in 20% of PMD patients. The clinical manifestations of patients with *PLP1* alterations are dependent on the genotypes.

Recently, we identified a rare *PLP1* triplication in a patient with PMD. In this study, we revealed the underlying genomic

organization with a duplication-inverted triplication-duplication (DUP-TRP/INV-DUP), which is a recently proposed mechanism of chromosomal rearrangement [2]. The clinical implication of *PLP1* gene dosage effects is discussed.

2. Materials, methods, and results

2.1. Clinical report

A 9-year-and-10-month-old boy was born at 38 weeks of gestation with a birth weight of 2400 g. Although his siblings were healthy, his maternal uncle and male cousin showed similar manifestations as his own; his maternal male cousin died at the age of 7 years (Supplemental Fig. S1). After birth, he showed nystagmus, laryngeal stridor, and profound hypotonia, and his subsequent psychomotor development was severely delayed. At the age of 5 months, his brain magnetic resonance imaging (MRI)

* Corresponding author.

E-mail addresses: toshiyukiyamamoto@twmu.ac.jp, yamamoto@imcir.twmu.ac.jp (T. Yamamoto).

revealed hypomyelination, which became profound at the age of 5 years and 5 months (Fig. 1).

At present, his height is 108 cm (<3rd centile), weight is 13.0 kg (<3rd centile), and head circumference is 47.7 cm (<3rd centile), indicating microcephaly. He shows severe developmental delay. He cannot turn over or sit on his own. Although he shows a lack of stable head control, he does not require head support when sitting in a “chair” position. He can eat minced food orally but with full support. Toilet habit is not acquired. He can vocalize, although very slowly, and can show his intentions by using simple signs or buttons. Mild scoliosis and mildly restricted range of movement in his hip and knee joints are noted. Neurological examination reveals mild muscular hypotonia. Pyramidal tract signs are prominent in his lower extremities; decreased deep tendon reflexes in his upper extremities, diminished abdominal reflex, increased deep tendon reflexes in his lower extremities, and positive Babinski reflex and ankle clonus in both his legs are also noted. Although some cerebellar signs are positive with continuous horizontal nystagmus and trunkal ataxia, the other findings are negative, including intention tremor and dysmetria. No dystonic finding is noted. Because he has never shown epileptic seizures, he has never been evaluated with electroencephalography. Moreover, no nerve conduction velocity tests have been done.

2.2. Cytogenetic analysis

From his clinical features, PMD was suspected as the candidate diagnosis. Then, we analyzed *PLP1* gene dosage by multiplex ligation-dependent probe amplification (MLPA) analysis, using Holland SALSA P022 MLPA probe mix (MRC Holland, Amsterdam, the Netherlands) according to the manufacturer’s protocol [7]. The peak height of *PLP1* in this patient was higher than that of previously evaluated patients with *PLP1* duplication, which led us to suspect triplication of *PLP1* rather than duplication (data not shown). To confirm this MLPA result, microarray-based comparative genomic hybridization (aCGH) analysis was performed using the Agilent catalog 105K oligonucleotide microarray (Agilent Technologies, Santa Clara, CA) according to the method described elsewhere [6], and the chromosomal aberration region was revealed to consist of duplicated and triplicated regions. To identify the precise aberration regions, a custom-made oligoarray was originally designed using the web-based software Agilent earray (<https://earray.chem.agilent.com/earray/>), according to the manufacturer’s protocol. The array included 11,526 probes between chrX

101,600,412–103,499,946 with an average interval of 147-bp (Agilent Technologies). Finally, genomic copy number gain was identified on Xq22.2 with a size of 984-kb (chrX: 102,321,416–103,305,265) in which a nested aberration of 214-kb including *PLP1* (chrX: 103,010,204–103,223,711) was included (Fig. 2A, Table 1).

The identified aberration was further examined by fluorescence *in situ* hybridization (FISH) as previously described [6]. Metaphase and interphase nuclei were prepared from peripheral blood lymphocyte-stimulated phytohemagglutinin according to the standard method. Human bacterial artificial clones were selected from the UCSC Genome Browser (<http://www.genome.ucsc.edu>) as described previously [6]. The results of FISH analysis were compatible with that of aCGH and confirmed that the triplicated region including *PLP1* was surrounded by duplicated regions (Fig. 2B–D). The patient’s mother declined examination for the carrier status of *PLP1* triplication.

The underlying genomic organization was investigated using long range PCR-based analyses with Tks Gflex™ DNA Polymerase (Takara, Ohtsu, Japan). The primers used for PCR are listed in Supplemental Table S1. The combinatory use of sense primers A and B generated an appropriately 20-kb PCR product, which fit the predicted architecture of junction 1 (Fig. 3A and B). The combinatory use of antisense primers C and D also generated a 756-bp PCR product (Fig. 3A and B). Direct sequencing analysis identified the junction 2 sequence (Fig. 3C). Because there is no homologous sequence in junction 2, this rearrangement was considered a consequence of non-homologous end-joining (NHEJ) [4].

3. Discussion

We presented a male patient with generalized spasticity, severe developmental delay, and hypomyelination. His condition was diagnosed as PMD on the basis of clinical findings. We detected *PLP1* triplication from combined examinations with MLPA, aCGH, and FISH analyses. aCGH analysis confirmed a duplicated region on Xq22.2 in which a nested aberration with triplicated region of *PLP1* was identified.

Recently, Carvalho et al. proposed a new mechanism for genomic rearrangement causing the genomic organization DUP-TRP/INV-DUP in 5 patients with *MECP2*-related disorders [2], in whom various sizes of triplicated segments were found embedded in the neighboring duplicated segments and were inserted in an inverted orientation. The existence of inverted repeats in the

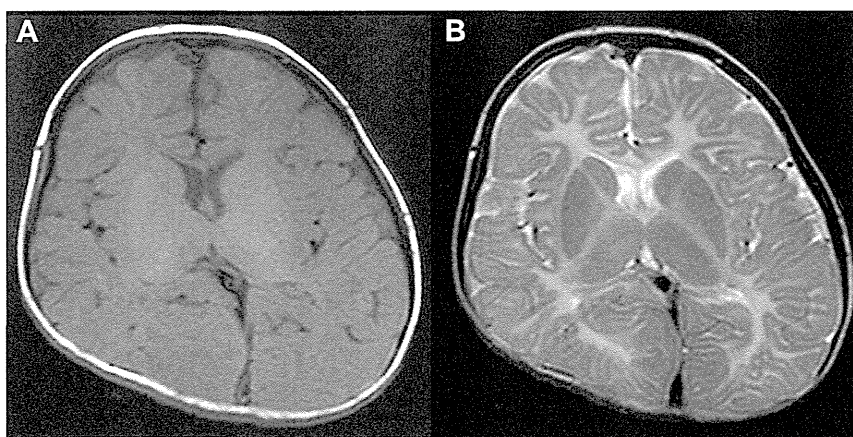


Fig. 1. Brain MRI of the patient performed at 5 years and 5 months of age. The reduction in the contrast of cortex and white matter in T1-weighted image (A) and the diffuse hyper-signal in T2-weighted image (B) show severe hypomyelination. Complete lack of myelination is also shown in the posterior limb of internal capsule.

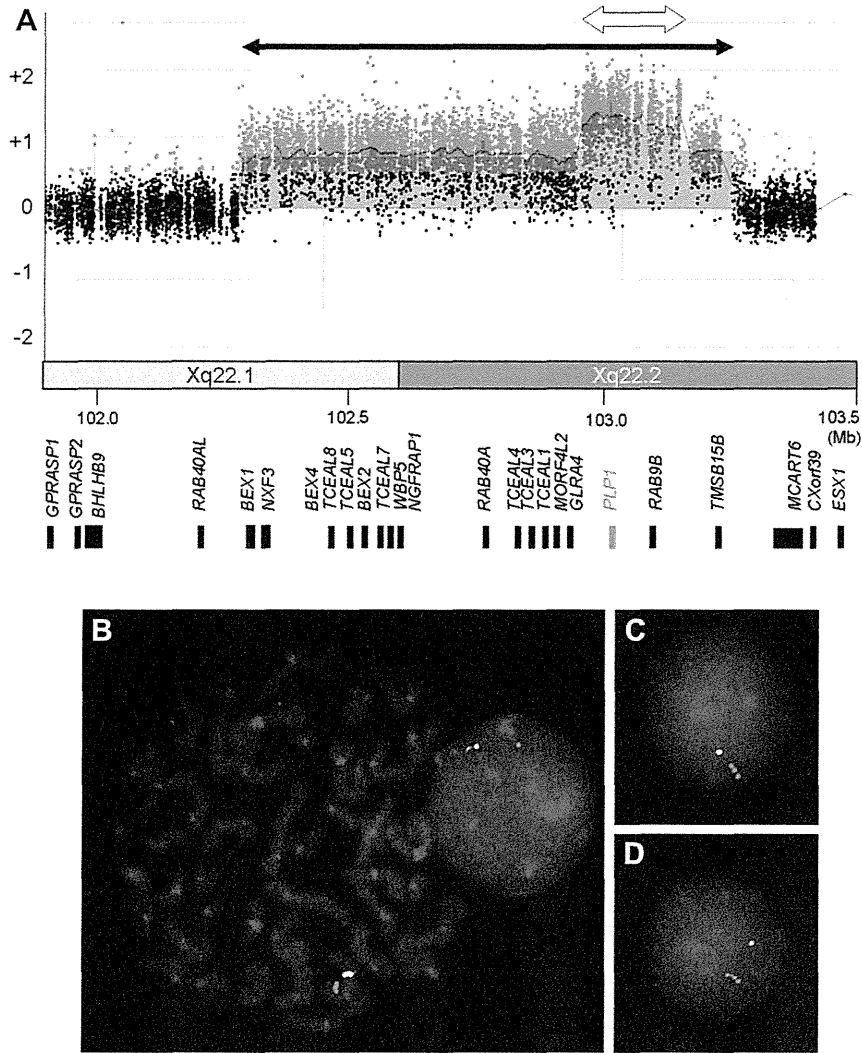


Fig. 2. Results of cytogenetic and molecular analyses. (A) The genome view of the result of custom array represents a chromosomal duplication (black bar with arrow on both ends) and a nested triplication including *PLP1* (white bar with arrow on both ends). (B) Two green signals of CTD-2086O16 (chrXq22.2: 102,807,623–102,897,468) were identified in the interphase nuclei, indicating duplication of this region. The red signal of RP11-75D20 (chrXp22.13: 18,314,474–18,506,931) was used as a marker. Both of the signals are on the same X chromosome, indicating that the *PLP1* locus is not translocated on the other chromosome. (C, D) Three red signals of RP4-540A13 (chrXq22.2: 103,067,273–10,3152,647) were identified in the interphase nuclei, indicating triplication of this region. The green signal of RP11-106N3 (chrXp22.13: 18,467,339–18,626,601) was used as a marker.

telomeric side mediates these inverted rearrangements [2]. Although the authors also identified a DUP-TRP/INV-DUP structure in the neighboring region of *PLP1* in one individual, the triplicated region did not include *PLP1* itself. In this study, we identified a DUP-TRP/INV-DUP structure in the present patient with PMD, and *PLP1* was included in the triplicated region. Detailed molecular examination revealed that two H2B histone family member X pseudogenes, *H2BFXP*, were located at each of the telomeric ends of the triplication and duplication (Fig. 3A). According to the UCSC Genome Browser, the two *H2BFXP* showed 99% identical sequences and were inserted in an inverted orientation (Fig. 3A). The result of this study indicated that the inverted orientation of *H2BFXP* mediated the first rearrangement (junction 1), and this caused the insertion of an inverted segment including *PLP1* and resulted as the triplication of this region. The 2nd rearrangement was caused by NHEJ [4], because there was no homologous sequence in junction 2 (Fig. 3C). From these results, the mechanism of the chromosomal

Table 1

The summary of the genomic copy number aberration

Chromosome band	Position	Average log ₂ ratio	Locus	
chrX	q22.1	0.76	CTD-2086O16	
				1.25
			RP4-540A13	
			<i>H2BFXP</i>	
	Primer A			
		Primer B		
	Primer C			
		Primer D		

Genomic position is referred to build 19

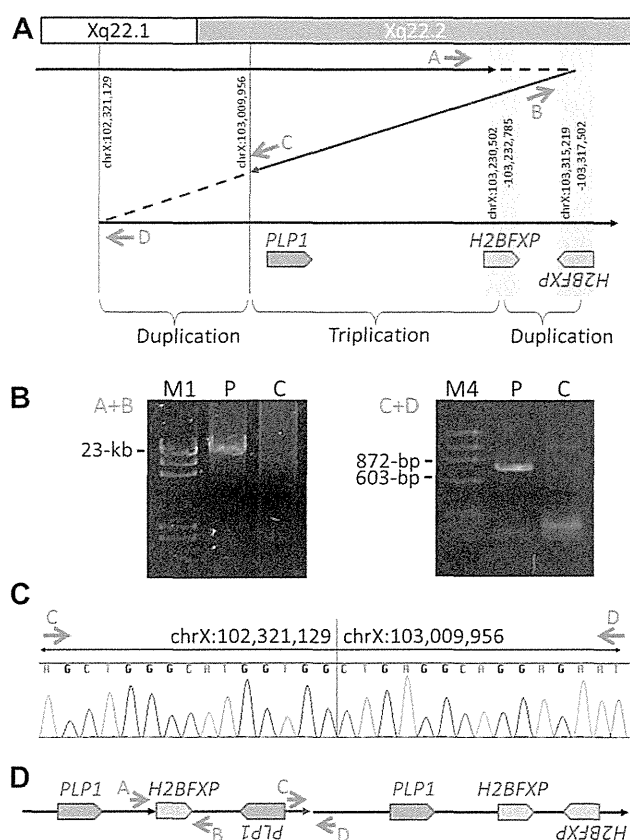


Fig. 3. Genomic organization of the present patient. (A) Predicted chromosomal rearrangements around Xq22.2. Red arrows, locations and directions of primers; trapezoids, locations and directions of genes; blue arrow, inverted genomic region. (B) Results of the electropherogram of the PCR products. The combinatory use of primers A + B generated an approximately 20-kb PCR product of junction 1, and primers C + D generated a 756-bp PCR product. M1, molecular marker of λ /HindIII digest; M4, molecular marker of ϕ X175/HaeIII digest; P, the present patient; C, normal control. (C) The sequencing electropherogram indicates junction 2, generated by PCR using primers C + D. (D) The final conclusion about the genomic organization is shown in the horizontal view.

rearrangement identified in this study can be explained by DUP-TRP/INV-DUP (Fig. 3D) [2].

Traditionally, PMD was classified into 3 categories: connatal form, classical form, and X-linked spastic paraplegia type 2 (SPG2; MIM#312920) [4]. Callioux et al. proposed a new subclassification of PMD as a continuous clinical spectrum [1]. According to these 2 classification systems, PMD patients with simple *PLP1* duplications manifest rather milder phenotypes (classical form/form 1–2), whereas PMD patients with nucleotide alterations often show severe phenotypes (connatal form/form 0). As the present patient has never achieved head control, his clinical condition can be traditionally classified as the connatal type and regarded as form 0 according to Callioux et al.'s classification [1]. However, he can eat

minced food orally and there is no strider at present. Thus, we regarded his condition as an intermediate form of PMD between classical (form 1) and connatal (form 0).

There have been only few reports of PMD patients with more than 2 copies of *PLP1* [3,5,8]. Five male patients with *PLP1* triplication reported by Wolf et al. showed severe clinical features compared with patients with *PLP1* duplications [8]. None of the 5 patients achieved stable head control, and their brain MRI showed an almost complete absence of the normal myelin signal [8]. The present patient also showed lack of stable head control, severe mental retardation, and a complete lack of myelination in the posterior limb of internal capsule was identified by brain MRI. Thus, our study gives evidence that patients with *PLP1* triplications show a more severe phenotype than patients with *PLP1* duplications.

Conflict of interest

The authors declare no conflict of interests.

Acknowledgements

This work was supported by Health Labor Sciences Research Grants from the Ministry of Health, Labor, and Welfare, Japan.

Appendix A. Supplementary data

Supplementary data associated with this article can be found, in the online version, at doi:10.1016/j.ejmg.2012.02.013.

References

- [1] F. Cailloux, F. Gauthier-Barichard, C. Mimault, V. Isabelle, V. Courtois, et al., Genotype-phenotype correlation in inherited brain myelination defects due to proteolipid protein gene mutations. *Clinical European Network on brain dysmyelinating disease*, *Eur. J. Hum. Genet.* 8 (2000) 837–845.
- [2] C.M. Carvalho, M.B. Ramocki, D. Pehlivan, L.M. Franco, C. Gonzaga-Jauregui, et al., Inverted genomic segments and complex triplication rearrangements are mediated by inverted repeats in the human genome, *Nat. Genet.* 43 (2011) 1074–1081.
- [3] P. Combes, M.N. Bonnet-Dupeyron, F. Gauthier-Barichard, R. Schiffmann, E. Bertini, et al., *PLP1* and *GPM6B* intragenic copy number analysis by MAPH in 262 patients with hypomyelinating leukodystrophies: identification of one partial triplication and two partial deletions of *PLP1*, *Neurogenetics* 7 (2006) 31–37.
- [4] K. Inoue, *PLP1*-related inherited dysmyelinating disorders: Pelizaeus-Merzbacher disease and spastic paraplegia type 2, *Neurogenetics* 6 (2005) 1–16.
- [5] J.A. Lee, C.M. Carvalho, J.R. Lupski, A DNA replication mechanism for generating nonrecurrent rearrangements associated with genomic disorders, *Cell* 131 (2007) 1235–1247.
- [6] K. Shimojima, T. Inoue, A. Hoshino, S. Kakiuchi, Y. Watanabe, et al., Comprehensive genetic analyses of *PLP1* in patients with Pelizaeus-Merzbacher disease applied by array-CGH and fiber-FISH analyses identified new mutations and variable sizes of duplications, *Brain Dev.* 32 (2010) 171–179.
- [7] I. Warshawsky, O.B. Chernova, C.A. Hubner, R. Stindl, M. Henneke, et al., Multiplex ligation-dependent probe amplification for rapid detection of proteolipid protein 1 gene duplications and deletions in affected males and carrier females with Pelizaeus-Merzbacher disease, *Clin. Chem.* 52 (2006) 1267–1275.
- [8] N.I. Wolf, E.A. Sistermans, M. Cundall, G.M. Hobson, A.P. Davis-Williams, et al., Three or more copies of the proteolipid protein gene *PLP1* cause severe Pelizaeus-Merzbacher disease, *Brain* 128 (2005) 743–751.
- [9] K.J. Woodward, The molecular and cellular defects underlying Pelizaeus-Merzbacher disease, *Expert Rev. Mol. Med.* 10 (2008) e14.



Case report

MR spectroscopy in 18q⁻ syndrome suggesting other than hypomyelination

Hiroko Tada^{a,*}, Jun-ichi Takanashi^{b,c}^a Department of Pediatrics, Chibaken Saiseikai Narashino Hospital, Narashino, Japan^b Department of Pediatrics, Kameda Medical Center, Kamogawa, Japan^c Department of Radiology, Toho University Sakura Medical Center, Sakura, Japan

Received 12 July 2012; received in revised form 17 September 2012; accepted 6 December 2012

Abstract

We reported a 5-year-old boy with 18q⁻ syndrome who showed typical magnetic resonance imaging (MRI) findings of high signal intensity on T2-weighted imaging, and a slightly high but lower than normal signal on T1-weighted imaging of the white matter. MR spectroscopy (MRS) revealed increased concentrations of creatine, myoinositol and choline with a normal *N*-acetylaspartate one. The cerebral white matter lesions observed on MRI in patients with 18q⁻ syndrome have been considered to reflect hypomyelination due to a decrease in myelin basic protein so far, however, MRS suggested reactive astrocytic gliosis and accelerated myelin turnover, which are compatible with recent pathological reports of 18q⁻ syndrome.

© 2012 The Japanese Society of Child Neurology. Published by Elsevier B.V. All rights reserved.

Keywords: 18q⁻ syndrome, MR spectroscopy; Hypomyelination; Gliosis; *MBP* gene

1. Introduction

18q⁻ syndrome is a rare chromosomal disorder involving frequent abnormal intensity of the white matter on T2-weighted imaging (T2WI) and the following clinical features: developmental delay, growth retardation, hearing loss, hypotonia, craniofacial dysmorphism, foot deformities, and eye movement disorders. Myelin basic protein (MBP) accounts for 30–40% of the total myelin protein in the central nervous system [1], and is thought to play an important role in myelin compaction. As the gene for MBP is encoded on 18q23, the region most commonly deleted in 18q⁻ syndrome [2,3], it has been considered that the magnetic resonance imaging (MRI) findings probably reflect hypomyelination due

to a haploinsufficiency of MBP [1]. We report a 5-year-old boy with 18q⁻ syndrome in whom quantitative MR spectroscopy (MRS) revealed increased choline (Cho), creatine (Cr), and myoinositol (mIns) concentrations. The increased Cho suggested accelerated myelin turnover rather than hypomyelination, and the increased Cr and mIns suggested astrocytic gliosis. The latter is compatible with a recent neuropathological report of 18q⁻ syndrome.

2. Case report

The patient, a 5-year-old Japanese boy, was delivered at 40 weeks gestation by means of vacuum extraction, weighing 3656 gm. He had no congenital cardiac disease or hearing loss. His motor and mental development were slow; he could only roll over at 6 months, sit alone at 9 months, and walk with support at 15 months and without support at 23 months. He did not utter any significant words at 2 years. G-Banding analysis revealed

* Corresponding author. Address: Department of Pediatrics, Chibaken Saiseikai Narashino Hospital, 1-1-1, Izumi-cho, Narashino City, Chiba 275-8580, Japan. Fax: +81 47 478 6601.

E-mail address: h.tada@hotmail.co.jp (H. Tada).

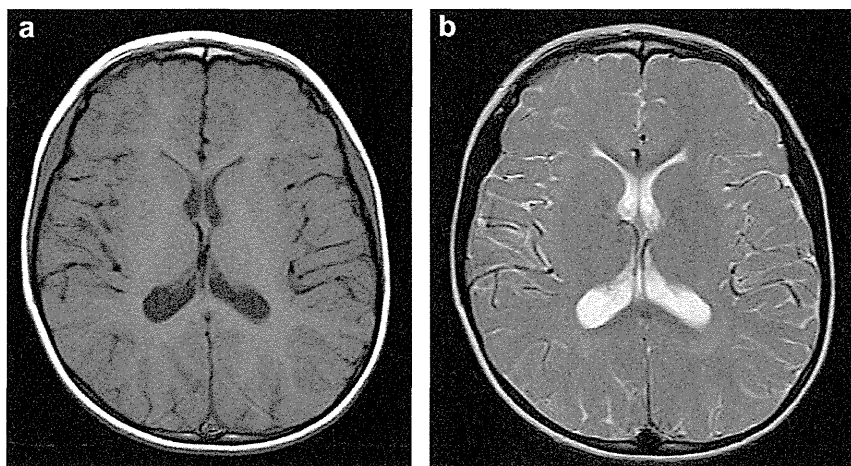


Fig. 1. (a) T1-weighted image showing the white matter exhibited higher intensity than the gray matter, but it was still lower than normal. (b) T2-weighted image showing the slightly high intensity in other white matter regions with poor gray and white matter contrast.

Table 1

Concentrations of metabolites (mM) determined with an LCModel in 18q⁻ syndrome.

	ROI	NAA	Cr	Cho	mIns
18q ⁻ syndrome	WM	7.66	4.76	1.72	4.26
Normal	WM	6.87 ± 0.59	3.59 ± 0.33	1.25 ± 0.11	3.13 ± 0.51

NAA, *N*-acetylaspartate; Cr, creatine; Cho, choline; mIns, myoinositol; ROI, region of interest; WM, white matter.

46, XY, del (18) (q21.3), leading to a diagnosis of 18q⁻ syndrome. His developmental questionnaire score was 46 at 5 years. He also presented with a short stature and craniofacial dysmorphism, such as a prominent forehead, brachycephaly, narrow eye clefts, hypertelorism, midface hypoplasia, epicanthal folds, a small upturned nose, and a carp-like mouth.

At 5 years, T1WI, T2WI and MRS (PRESS TR/TE = 5000/30) were performed with a 1.5 T Siemens apparatus. The concentrations of metabolites were quantitated with an LCModel using the modified water scaling method as previously reported [4]. On T1WI, the white matter exhibited slightly higher intensity than the gray matter, but it was still lower than normal (Fig. 1). T2WI showed low intensity in the corpus callosum, but slightly high intensity in the other white matter regions with poor gray and white matter contrast (Fig. 1). MRS revealed increased concentrations of Cho, Cr and mIns with a normal *N*-acetylaspartate (NAA) (Table 1 and Fig. 2).

3. Discussion

This is the first report of increased Cho observable on MRS in a patient with 18q⁻ syndrome, suggesting the underlying pathology is other than hypomyelination with reduced Cho. MR-visible Cho is derived from various cell membrane precursors and breakdown prod-

ucts, such as phosphocholine, glycerophosphocholine, and phosphatidylcholine, reflecting myelin metabolism, therefore, the Cho level increases during the newborn period, when myelin sheaths are actively being formed [5,6], and the acute phase of demyelination. MRS in patients with Pelizaeus-Merzbacher disease (PMD), a representative hypomyelination disorder, shows decreased Cho reflecting hypomyelination, that is, an absence of myelin and mature oligodendrocytes [5,6]. On the other hand, a recent neuropathological study on a patient with 18q⁻ syndrome revealed prominent astrogliosis, and normal myelinated fibers were observed on microscopical examination, which is distinct from in PMD. Immunohistological examination revealed normal immunoreactivity for MBP in myelinated fibers, but reduced immunoreactivity in oligodendrocytes [7]. Some functional abnormalities of oligodendrocytes may result in the increased myelin turnover and increase in Cho observable on MRS.

Shiverer mice with an abnormal *mbp* gene (*mbp* ^{-/-}) showed little or no myelination in a neuropathological study, and diffuse T2 prolongation in the white matter on MRI [8]. On the other hand, heterozygous mice (*mbp* ^{+/-}) show normal myelin sheaths and normal MRI findings [8], despite the presence of only half the normal amount of *mbp* protein. The heterozygous mice also show no clinical symptoms, however, the visually evoked potential (VEP) latency has been reported to

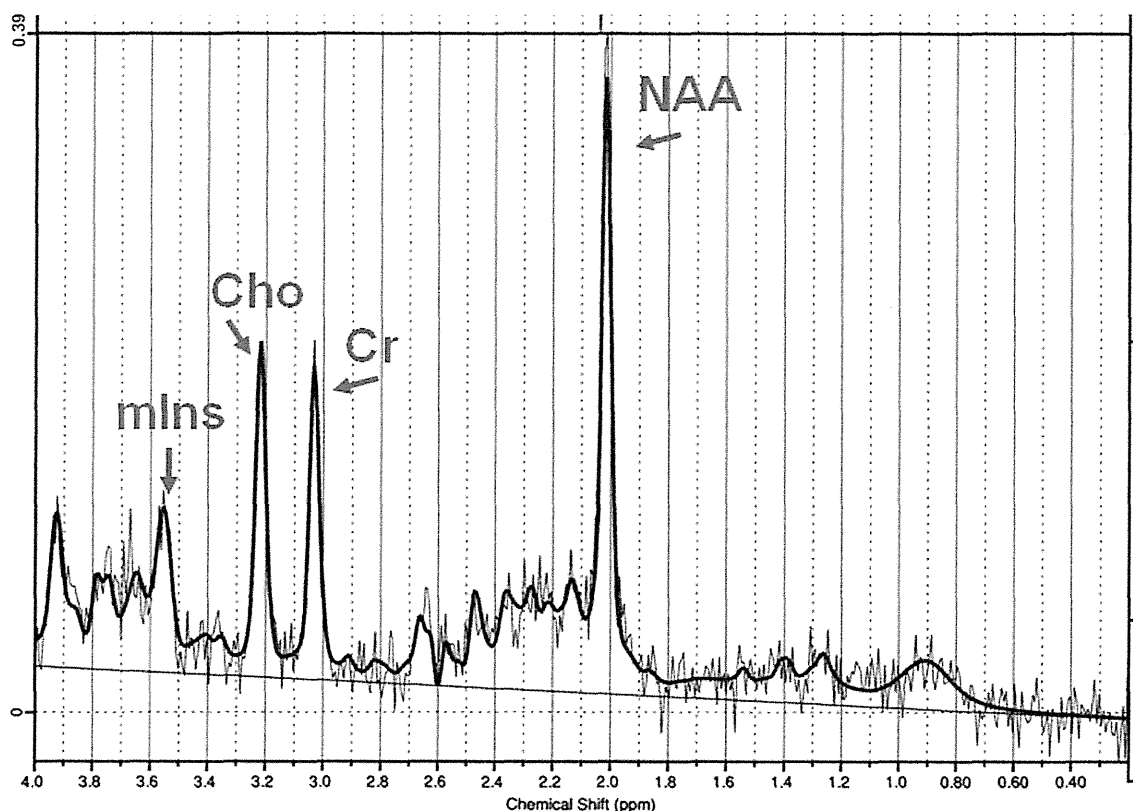


Fig. 2. MRS of the left white matter showing elevated Cho, Cr and mIns.

be increased [8], suggesting a dysfunction of the optic nerves. This might support our hypothesis for 18q⁻ syndrome that a dysfunction of oligodendrocytes and myelinated fibers may result in increased turnover of myelin and increased Cho. MRS of heterozygous mice (*mbp* +/-) would allow more accurate assessment of the hypothesis.

Increased mIns, which is abundant in astrocytes, is considered to reflect astrogliosis [5,6]. Cr is more concentrated in glia than in neurons, and is also expected to be increased in astrogliosis [5]. Increases in Cr and mIns in 18q⁻ syndrome would, therefore, reflect astrogliosis, as shown by a recent pathological study [7]. We speculate that the astrogliosis results in T2 prolongation in the white matter. Because heterozygous mice show no astrogliosis (unpublished data), it is speculated that a broad gene deletion in patients with 18q⁻ syndrome includes not only the *MBP* gene, but also another gene or genes causing astrogliosis, that is, 18q⁻ syndrome is a contiguous gene syndrome.

To our knowledge, there has been only one report of MRS in a patient with 18q⁻ syndrome, which showed increased Cho/Cr at 30-months-old, followed by a decrease in it during follow-up [9]. Because the Cr concentrations remains relatively constant in the brain in different metabolic conditions, it is often used as a refer-

ence to measure NAA and Cho, however, altered concentrations of Cr have been reported [4], as observed in this patient. Therefore, normalizing the Cho value as to Cr would be inappropriate and lead to misunderstanding of the results, especially when both are increased. To resolve this problem, we performed absolute quantification of the metabolite with an LCModel, which confirmed the increased concentration of Cho.

In conclusion, the results of MRS in a patient with 18q⁻ syndrome suggest increased myelin turnover and gliosis, and not the hypomyelination previously considered.

Acknowledgements

This study was supported in part by a Grant-in-aid for Research on Measures for Intractable Diseases (H24-Nanchi-Ippan-72), and a Research Grant for Nervous and Mental Disorders (24-7), both from the Ministry of Health, Labor and Welfare of Japan; and by a Grant-in-Aid for Scientific Research (C-24591790) from the Japan Society for the Promotion of Science.

References

- [1] van der Knaap MS, Valk J. 18q⁻ syndrome. In: van der Knaap MS, Valk J, editors. Magnetic resonance of myelination and myelin disorders. Heidelberg, Germany: Springer; 2005. p. 281–3.

- [2] Gay CT, Hardies LJ, Rauch RA, Lancaster JL, Plaetke R, DuPont BR, et al. Magnetic resonance imaging demonstrates incomplete myelination in 18q⁻ syndrome: evidence for myelin basic protein haploinsufficiency. *Am J Med Genet* 1997;74:422–31.
- [3] Hale DE, Cody JD, Baillargeon J, Schaub R, Danney MM, Leach RJ, et al. The spectrum of growth abnormalities in children with 18q deletions. *J Clin Endocrinol Metab* 2000;85:4450–4.
- [4] Takanashi J, Somazawa F, Maruyama K, Terada H, Xu D, Barkovich AJ. Metabolic changes in early childhood using LCMoDel with corrected water scaling method. *J Magn Reson Imaging* 2012;35:174–80.
- [5] Takanashi J, Saito S, Aoki I, Barkovich AJ, Ito Y, Inoue K. Increased *N*-acetylaspartate in model mouse of Pelizaeus-Merzbacher disease. *J Magn Reson Imaging* 2012;35:418–25.
- [6] Takanashi J, Inoue K, Tomita M, Kurihara A, Morita F, Ikehira H, et al. Brain *N*-acetylaspartate is elevated in Pelizaeus-Merzbacher disease with PLP1 duplication. *Neurology* 2002;58:237–41.
- [7] Tanaka R, Iwasaki N, Hayashi M, Nakayama J, Ohto T, Takahashi M, et al. Abnormal brain MRI signal in 18q⁻ syndrome not due to dysmyelination. *Brain Dev* 2012;34:234–7.
- [8] Martin M, Hiltner TD, Wood JC, Fraser SE, Jacobs RE, Readhead C. Myelin deficiencies visualized in vivo: visually evoked potentials and T2-weighted magnetic resonance images of shiverer mutant and wild-type mice. *J Neurosci Res* 2006;84:1716–26.
- [9] Häusler M, Anhof D, Schüller H, Ramaekers VT, Thron A, Zerres K, et al. White-matter disease in 18q deletion (18q⁻) syndrome: magnetic resonance spectroscopy indicates demyelination or increased myelin turnover rather than dysmyelination. *Neuroradiology* 2005;47:83–6.

Depletion of Molecular Chaperones from the Endoplasmic Reticulum and Fragmentation of the Golgi Apparatus Associated with Pathogenesis in Pelizaeus-Merzbacher Disease*

Received for publication, November 13, 2012, and in revised form, January 23, 2013. Published, JBC Papers in Press, January 23, 2013, DOI 10.1074/jbc.M112.435388

Yurika Numata^{‡§}, Toshifumi Morimura^{‡¶}, Shoko Nakamura[‡], Eriko Hirano[‡], Shigeo Kure[§], Yu-ich Goto[‡], and Ken Inoue^{‡¶1}

From the [‡]Department of Mental Retardation and Birth Defect Research, National Institute of Neuroscience, National Center of Neurology and Psychiatry (NCNP), 4-1-1 Ogawahigashi-machi, Kodaira-shi, Tokyo 187-8502, the [§]Department of Pediatrics, Tohoku University School of Medicine, 1-1 Seiryomachi, Aobaku, Sendai 980-8574, and the [¶]Unit for Neurobiology and Therapeutics, Molecular Neuroscience Research Center, Shiga University of Medical Science, Seta-Tsukinowa-cho, Otsu, Shiga 520-2192, Japan

Background: Mutations of proteolipid protein 1 (*PLP1*) induce endoplasmic reticulum (ER) stress.

Results: PLP1 mutants deplete some chaperones from the ER and induce fragmentation of the Golgi apparatus (GA).

Conclusion: These changes affect clinical pathology in disease-causing mutations of *PLP1*.

Significance: This work provides a novel insight involving global changes of organelles in pathogenesis of ER stress-related diseases.

Missense mutations in the proteolipid protein 1 (*PLP1*) gene cause a wide spectrum of hypomyelinating disorders, from mild spastic paraplegia type 2 to severe Pelizaeus-Merzbacher disease (PMD). Mutant PLP1 accumulates in the endoplasmic reticulum (ER) and induces ER stress. However, the link between the clinical severity of PMD and the cellular response induced by mutant PLP1 remains largely unknown. Accumulation of misfolded proteins in the ER generally leads to up-regulation of ER chaperones to alleviate ER stress. Here, we found that expression of the PLP1-A243V mutant, which causes severe disease, depletes some ER chaperones with a KDEL (Lys-Asp-Glu-Leu) motif, in HeLa cells, MO3.13 oligodendrocytic cells, and primary oligodendrocytes. The same PLP1 mutant also induces fragmentation of the Golgi apparatus (GA). These organelle changes are less prominent in cells with milder disease-associated PLP1 mutants. Similar changes are also observed in cells expressing another disease-causing gene that triggers ER stress, as well as in cells treated with brefeldin A, which induces ER stress and GA fragmentation by inhibiting GA to ER trafficking. We also found that mutant PLP1 disturbs localization of the KDEL receptor, which transports the chaperones with the KDEL motif from the GA to the ER. These data show that PLP1 mutants inhibit GA to ER trafficking, which reduces the supply of ER chaperones and induces GA fragmentation. We propose that depletion of ER chaperones and GA fragmentation induced by mutant misfolded proteins contrib-

ute to the pathogenesis of inherited ER stress-related diseases and affect the disease severity.

A number of inherited human diseases are caused by missense mutations. These mutations in the membrane and secretory proteins often lead to improper protein folding and accumulation in the endoplasmic reticulum (ER),² resulting in an induction of ER stress. In cells under ER stress, accumulation of mutant proteins in the ER activates the unfolded protein response (UPR), which initiates a block in translation, increases retrotranslocation and degradation of ER-localized proteins, and bolsters the protein-folding capacity of the ER (1, 2). Through these processes, the UPR functions as a cellular quality control system that essentially protects cells from the toxicity of accumulated proteins in the ER. The UPR is activated by three distinct pathways, activating transcription factor 6 (ATF6), inositol-requiring kinase 1 (IRE1), and protein kinase-like ER kinase (3), all of which are negatively regulated by interaction with the 78-kDa glucose-regulated protein (GRP78, also referred to as BiP/HSPA5). On accumulation of unfolded protein, GRP78 binds to unfolded proteins and dissociates from

² The abbreviations used are: ER, endoplasmic reticulum; PLP1, proteolipid protein 1; PMD, Pelizaeus-Merzbacher disease; msd, myelin synthesis deficit; SPG2, spastic paraplegia type 2; msd, myelin synthesis deficit; GA, Golgi apparatus; PDI, protein-disulfide isomerase; CALR, calreticulin; GRP78, glucose-regulated protein of 78 kDa; CANX, calnexin; MBP, myelin basic protein; UPR, unfolded protein response; ATF6, activating transcription factor 6; IRE1, inositol-requiring kinase 1; XBP1, X-box protein 1; CHOP, C/EBP homologous protein; ALS, amyotrophic lateral sclerosis; MPZ, myelin protein zero; PMP22, peripheral myelin protein 22; CMT, Charcot-Marie-Tooth disease; SC, spinal cords; TUNEL, terminal deoxynucleotidyl transferase dUTP nick end labeling; MGC, mixed glial culture; BFA, brefeldin A; MOG, myelin oligodendrocyte glycoprotein; GFP, green fluorescent protein; luc, luciferase; RLuc, *Renilla* luciferase; Igκ, immunoglobulin κ light chain; Cluc, cytoplasmic luciferase; DMSO, dimethyl sulfoxide.

* This work was supported in part by grants from the Health and Labor Sciences Research Grants, Research on Intractable Diseases H24-Nanchitoulppan-072 (to K. I.), a grant from Takeda Science Foundation (to K. I.), and Grants-in-Aid for Scientific Research from the Ministry of Education, Culture, Sports, Science and Technology, Japan, KAKENHI: 21390103 and 23659531 (to K. I.) and 23580417 (to T. M.).

¹ To whom correspondence should be addressed. Tel.: 81-42-346-1713; Fax: 81-42-346-1743; E-mail: kinoue@ncnp.go.jp.

Depletion of ER Chaperones and GA Fragmentation in PMD

the ER stress sensors, which trigger the UPR (3). ATF6 induces transcription of major ER chaperones and X box-binding protein 1 (*XBPI*) (4). The endonuclease activity of IRE1 splices *XBPI* (5), which functions as a transcription factor that drives the expression of UPR-related genes (4). The ATF6 and IRE1-*XBPI* axes promote the expression of ER chaperones that facilitate the correct folding or assembly of ER proteins and prevent their aggregation, thereby improving cell survival (3, 4, 6). However, when ER stress overwhelms the capacity of this intrinsic quality control, apoptosis is induced by up-regulation of the C/EBP homologous protein (CHOP).

In inherited diseases associated with ER stress, different mutations in the causative genes result in various phenotypes. One representative example, Pelizaeus-Merzbacher disease (PMD), is an X-linked recessive leukodystrophy characterized by diffuse hypomyelination in the central nervous system (CNS) (7). Missense mutations in the proteolipid protein 1 (*PLP1*) gene cause a wide spectrum of clinical phenotypes from a mild allelic disease, spastic paraplegia type 2 (SPG2) to severe congenital PMD (7). In these diseases, mutant proteins are misfolded and accumulate in the ER, leading to induction of ER stress and apoptosis of oligodendrocytes in the CNS (8, 9). However, little is known about how different mutations in the same gene induce ER stress differently and affect clinical severity. Factors, such as retention of misfolded proteins or the extent of UPR activation, may influence phenotypic variation (9–11). However, can any other factors contribute to the pathology of such ER stress-related disease? Here we focused on ER chaperones as a potential player. ER chaperones are highly conserved proteins that assist in protein folding. Therefore, it is generally believed that accumulation of misfolded proteins in the ER up-regulates chaperones to alleviate ER stress. In terms of its association with disease pathology, interaction between the mutant *PLP1* and a major ER chaperone, calnexin (*CANX*), was shown to inhibit degradation of the misfolded mutant proteins (12). In the mutant superoxide dismutase model of amyotrophic lateral sclerosis (ALS), an ER stress-associated neurodegenerative disease, down-regulation of another chaperone, calreticulin (*CALR*), was shown to induce ER stress and trigger the death of mutant superoxide dismutase motoneurons (13). A recent study reported up-regulation of protein-disulfide isomerase (*PDI*, also referred to as *P4HB*), which is a chaperone in the ER catalyzing the formation and breakage of protein disulfides bonds, in microglia of transgenic mutant superoxide dismutase 1 mice (14). Therefore, we sought to determine whether changes in the expression of ER chaperones alter the accumulation of misfolded protein and ER stress, potentially modifying the cellular and clinical phenotypes.

For this purpose, we used PMD as a model and investigated missense *PLP1* mutations (8, 11). *PLP1* with an A243V substitution (*PLP1msd*) is representative of the severe hypomyelination in myelin synthesis deficit (*msd*) mice (15) and humans (16), whereas two other mutations, W163L and I187T, are representative of the milder condition found in mild PMD/SPG2 patients (17, 18): the latter is also the mutation found in an SPG2 mouse model, *rumpshaker* (19). We also employed mutants in two other genes responsible for peripheral myelin

disorders, a myelin protein zero (*MPZ*) mutant associated with a severe neuropathy, Dejerine-Sottas neuropathy (20), and two peripheral myelin protein 22 (*PMP22*) mutants that are associated with a clinically mild neuropathy, Charcot-Marie-Tooth disease (21–23).

In this study, we examined the expression of ER chaperones in response to mutants of *PLP1* and two other genes. Unexpectedly, we found that some ER chaperones were depleted rather than up-regulated. In addition, these mutant proteins induced fragmentation of the Golgi apparatus (GA). We also found an association between these changes and phenotypic severity. Furthermore, we proposed potential mechanisms underlying these cellular phenotypes. The results of this study suggest that changes in these subcellular organelles may contribute to the cellular pathogenesis and phenotypic severity of inherited ER stress-related diseases caused by mutant proteins.

EXPERIMENTAL PROCEDURES

Mice—*Msd* mice, which carry the spontaneous A243V mutation in the *Plp1* gene (15), were maintained in a B6C3F1/J background in accordance with the institutional guidelines of the National Center of Neurology and Psychiatry.

Plasmid Construction—Expression vectors for *PLP1wt* and *PLP1msd* were reported previously (24). *PLP1-W163L* and *PLP1-I187T* genes were generated by site-directed mutagenesis with modifications (25), and subcloned into pCAGGS (24), as fusions with N-terminal FLAG epitopes. Human wild-type and mutant *PMP22* and *MPZ* genes were amplified from cloned cDNAs (kind gift from Dr. JR Lupski) using appropriate primers and inserted into pCAGGS. For construction of an expression vector for the membrane-linked cell surface green fluorescent protein (GFP) as illustrated in Fig. 9E. The *GFP* gene was inserted into pDisplay (Invitrogen) in an in-frame manner. The *cytoplasmic luciferase (Cluc)* and *immunoglobulin (Ig) κ light chain (Igκ-Rluc)* genes were amplified from cloned cDNA (Promega) with appropriate primers, and cloned into pCDNA3.1 (Invitrogen) and pAP-Tag5 (GenHunter) to construct pCMV-*Cluc* and pCMV-*Igκ-Rluc*, respectively. To determine subcellular localization, the *Rluc* gene was inserted in-frame between the *Igκ* and *myc* sequences of pAP-Tag5 to make pCMV-*Igκ-Rluc-Myc*. The mouse myelin oligodendrocyte glycoprotein (*MOG*) gene was also amplified with appropriate primers using cDNA from postnatal day (P) 14-mouse spinal cord (SC), and cloned into pEGFP-N1 (Takara).

Chemicals and Antibodies—The following reagents were purchased from the suppliers indicated: brefeldin A (Wako), tunicamycin (Merck), thapsigargin (Sigma), lactacystin (Wako), and MG132 (Wako). The primary antibodies included mouse anti-*PDI* (Thermo Scientific, MA3-019), rabbit anti-*CALR* (Sigma, C4606), rabbit anti-*GRP78* (Abcome, ab21685), rabbit anti-*CANX* (Enzo Life Sciences, ADI-SPA-860), mouse anti-*CHOP* (Santa Cruz Biotechnology, sc-7351), rabbit anti-*GM130* (Abcome, ab52649), mouse anti-FLAG M2 (Sigma, F3165), rabbit anti-FLAG M2 (Cell Signaling, number 2368), mouse anti-c-Myc (Nacalai Tesque, MC045), rabbit anti-*PLP* (a kind gift from Dr. M. Itoh, NCNP), rabbit anti-*Oligo2* (IBL 18953), mouse anti-myelin basic protein (*MBP*) (Covance, SMI-99P), mouse anti-action (Millipore, MAB1501), rabbit

AQ: A

AQ: B

Depletion of ER Chaperones and GA Fragmentation in PMD

anti-KDEL receptor (Santa Cruz Biotechnology, sc-33806) and mouse anti-ubiquitin (Santa Cruz Biotechnology, sc-8017) antibodies. Alexa Fluor-488, -594, and -647 secondary antibodies were purchased from Invitrogen. Horseradish peroxidase-labeled anti-mouse and rabbit antibodies were purchased from GE Healthcare.

Cell Culture—HeLa cells and human oligodendrocytic cells (MO3.13) were maintained in Dulbecco's modified Eagle's medium (DMEM, Thermo Scientific) supplemented with 20 units ml⁻¹ of penicillin, 20 μg ml⁻¹ of streptomycin, and 10% fetal bovine serum. For transfection, HeLa cells were plated onto 6-well plates or 18-mm round coverslips in 12-well plates, and transfected with the indicated constructs using Lipofectamine 2000 (Invitrogen) or TransIt LT1 (Mirus), respectively, according to the manufacturers' protocols. After 24 h, transfected cells in the 6-well plates or on coverslips were subjected to immunoblotting, quantitative PCR and immunocytochemistry, respectively.

Mixed Glial Culture (MGC) Generated to Oligodendrocyte—MGCs were established from wild-type and *msd* mice, which were then differentiated into oligodendrocytes, as described by Abematsu *et al.* (26).

Immunoblot Analysis—HeLa cells and mouse SCs were lysed with TNE(+) lysis buffer (50 mM Tris-HCl, pH 8.0, 150 mM NaCl, 2 mM EDTA, 1% Triton-X-100, and 0.1% SDS) supplemented with protease and phosphatase inhibitors on ice for 10 min. For the digitonin fractionation experiment, HeLa cells were permeabilized with phosphate-buffered saline (PBS) containing 0.01% digitonin with protease and phosphatase inhibitors on ice for 10 min. After soluble proteins were collected, insoluble proteins were further treated with the TNE(+) lysis buffer. These extracts were centrifuged at 12,000 × *g* for 10 min to remove cell debris. Co-immunoprecipitation and cell surface biotinylation were performed as described previously (27). The cell extracts, co-immunoprecipitation and biotinylated samples, were subjected to immunoblotting with primary antibodies and horseradish peroxidase-labeled secondary antibodies. All immunoblot analyses were repeated at least 3 times with similar results. The relative protein expression levels on immunoblotting were quantified by an image analyzer.

Immunocytochemistry—HeLa cells, MO3.13 cells, and primary oligodendrocytes were fixed with 4% paraformaldehyde in PBS for 10 min, permeabilized with 0.1% Triton X-100 for 10 min, and treated with 3% bovine serum albumin to block non-specific reaction. Detection of cell surface proteins, cells were not permeabilized by 0.1% TritonX-100. Cells were further incubated with the primary antibodies for 60 min at RT followed by visualization using the appropriate secondary antibodies labeled with Alexa-488, -594, or -647 with 4',6-diamidino-2-phenylindole (DAPI). Apoptotic cells were detected using ApopTag kit (Chemicon), according to the manufacturer's protocol. These stained cells were observed with a confocal fluorescence microscope (FV-1000; Olympus).

Quantitative Reverse Transcriptase-Polymerase Chain Reaction—Total RNA was extracted from HeLa cells and mouse SCs and was converted to cDNA using SuperScript III reverse transcriptase (Invitrogen). Transcript levels were analyzed by a thermal cycler (7900HT; Applied Biosystems) with

synthesized cDNA and the following pre-designed TaqMan probes (Applied Biosystems): human *GAPDH*, Hs99999905; human *CHOP*, Hs00358796; human *P4HB*, Hs00168586; human *CALR*, Hs00189032; human *GRP78*, Hs99999174; human *CANX*, Hs00233492; mouse *Gapdh*, Mm99999915; mouse *Chop*, Mm00492097; mouse *P4hb*, Mm01243184; mouse *Calr*, Mm00482936; mouse *Grp78*, Mm00517691; and mouse *Canx*, Mm00500330. Relative transcript levels were calculated by the $\Delta\Delta C_T$ method according to the manufacturer's standard protocol.

Luciferase Reporter Assay—HeLa cells were co-transfected with the Cluc and Igκ-Rluc genes along with pCDNA3.1-PLP1wt-FLAG, pCDNA3.1-PLP1msd-FLAG, or the empty vector. Activities for firefly luciferase and Igκ-Rluc in the cell lysate and supernatant were measured using a dual-luciferase assay system (Promega) according to the manufacturer's instructions. Relative Cluc and Igκ-Rluc activities in the supernatant were determined as ratios to cytosolic luciferase activity.

Statistical Analysis—Student's *t* test and analysis of variance were used for statistical analyses.

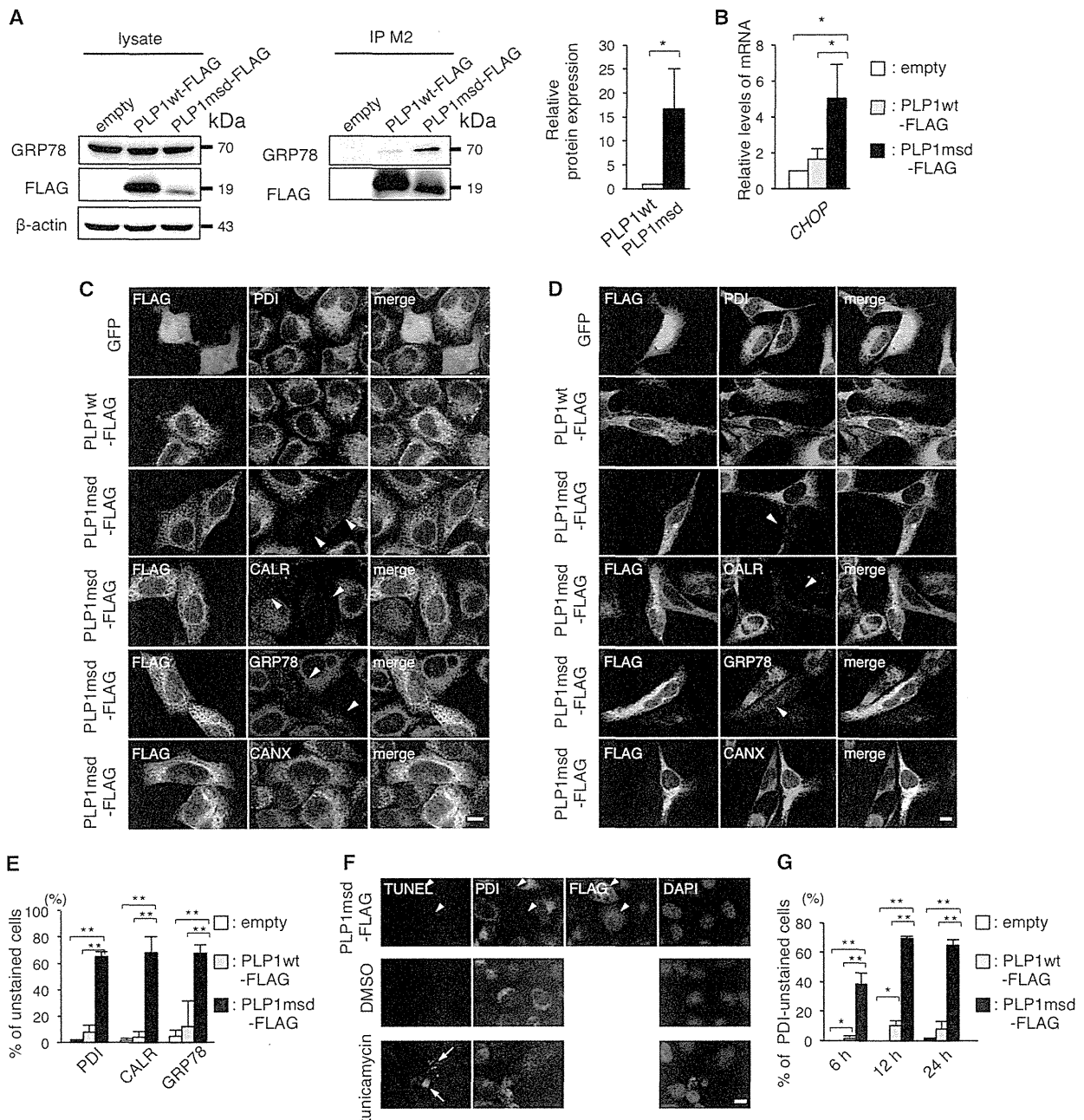
RESULTS

PDI, CALR, and GRP78 Are Depleted in the ER of HeLa Cells

Expressing PLP1msd—Typically, when cells are under ER stress, ER chaperones are up-regulated as a part of the UPR. ER chaperones improve cell survival by facilitating the correct folding or assembly of misfolded proteins and preventing their aggregation (28). In HeLa cells, FLAG-tagged PLP1msd (PLP1msd-FLAG), a PMD-causing severe mutant known to induce ER stress (8) but not FLAG-tagged wild-type PLP1 (PLP1wt-FLAG), effectively co-immunoprecipitated GRP78 (Fig. 1A) and up-regulated the *CHOP* gene (Fig. 1B), a well characterized ER stress marker gene, indicating that this transient transfection system is applicable for analyzing cellular pathogenesis of ER stress caused by exogenous mutant proteins. To further analyze the changes in ER chaperone expression induced by this mutant PLP1, transfected HeLa cells were immunostained with antibodies against the FLAG epitope, PDI, CALR, GRP78, and CANX. Unexpectedly, we found that PDI, CALR, and GRP78 were drastically depleted, whereas CANX expression was unchanged (Fig. 1C). These changes were also observed in the human oligodendrocytic cell line MO3.13 (Fig. 1D), the human glioma cell line U-138, and simian kidney cell line COS-7 cells (data not shown). Almost 65% of the cells transfected with PLP1msd-FLAG had faint PDI, CALR, and GRP78 staining. This proportion was significantly higher than in cells transfected with PLP1wt-FLAG (Fig. 1E), suggesting that this phenomenon is due to the mutant PLP1, not the overexpression of PLP1 itself.

Next, we determined if reduced chaperone expression is caused by apoptotic cell death due to overwhelming ER stress. Cells expressing PLP1msd that had faint PDI immunostaining had no positive signal in the terminal deoxynucleotidyl transferase dUTP nick-end labeling (TUNEL) assay (Fig. 1F). Furthermore, depletion of PDI occurred as early as 6 h after transfection (Fig. 1G). These results suggest that PLP1msd impairs the ER chaperones independent of apoptosis.

Depletion of ER Chaperones and GA Fragmentation in PMD



AQ: F FIGURE 1. **PLP1msd overexpression resulted in a negative ER chaperone staining pattern.** *A*, co-immunoprecipitation of PLP1 with GRP78 in HeLa cells. *B*, quantitative RT-PCR for the *CHOP* gene in HeLa cells expressing PLP1wt or PLP1msd. The *GAPDH* gene was used as an internal control. Results are represented as fold-induction compared with empty vector-transfected control experiment. Values are represented as the mean \pm S.E. from three independent experiments (*, $p \leq 0.05$). *C* and *D*, immunocytochemistry of ER chaperones in HeLa cells (*C*) and human oligodendrocytic cells, and MO3.13 cells (*D*) expressing PLP1wt or PLP1msd. Cells transfected with the indicated vectors were immunostained with an anti-FLAG antibody (green) together with anti-PDI, anti-CALR, anti-GRP78, or anti-CANX antibodies (magenta) and observed with a confocal fluorescence microscope. Note that cells expressing PLP1msd showed an extremely faint staining pattern (arrowheads) for PDI, CALR, and GRP78, but not for CANX. Scale bar, 10 μ m. *E*, the proportion of unstained cells for PDI, CALR, and GRP78. *F*, apoptosis of HeLa cells expressing PLP1msd. TUNEL assay combined with immunocytochemical staining using the anti-FLAG (white) and anti-PDI (magenta) antibodies. Tunicamycin treatment served as a positive control for TUNEL (arrow). None of the PLP1msd-positive cells showed positive signals for TUNEL (arrowheads). Scale bar, 10 μ m. *G*, time course of the proportion of PDI negative HeLa cells transfected with the PLP1msd gene. The results are represented as the mean \pm S.E. from three independent experiments with >100 cells counted in each experiment (*, $p \leq 0.05$; **, $p \leq 0.005$).

Expression of PLP1msd Translocates the ER Chaperones from the ER—To examine whether PLP1msd depletes the chaperones by inhibiting their transcription in HeLa cells, we performed quantitative real time-polymerase chain reaction (RT-PCR) (Fig. 2A). As we demonstrated previously (24), GRP78

mRNA expression was increased significantly in cells transfected with PLP1msd-FLAG compared with cells transfected with PLP1wt-FLAG. The expression of PDI and CALR was slight, but significantly up-regulated. These results indicate that PDI, CALR, and GRP78 are depleted in the ER without

F2

Depletion of ER Chaperones and GA Fragmentation in PMD

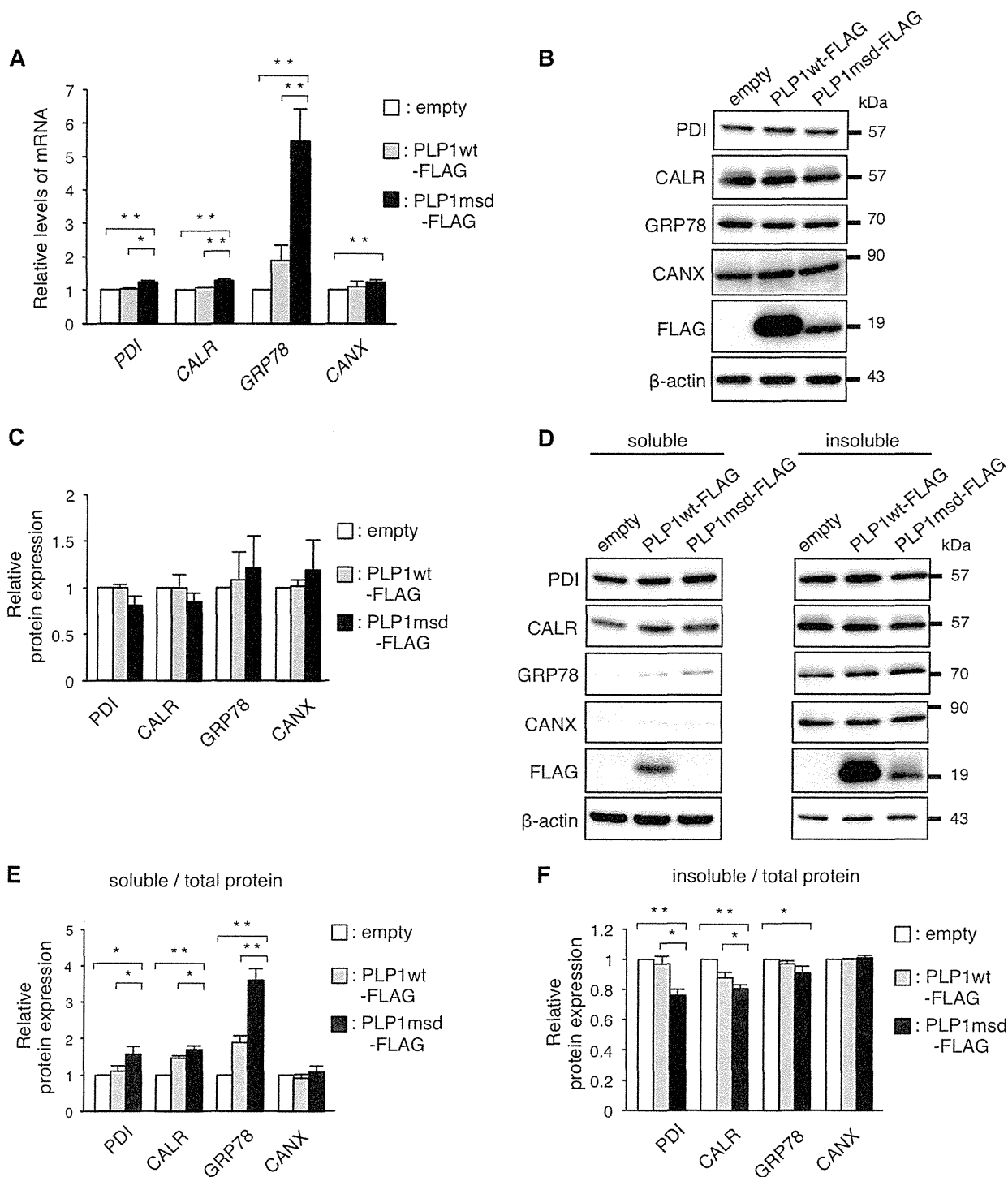


FIGURE 2. PDI, CALR, and GRP78 are depleted from the ER without decreasing their transcripts. A, relative expression of the transcripts of the ER chaperones in HeLa cells transfected with the PLP1 genes. Expression levels of PDI, CALR, GRP78, and CANX mRNA were analyzed by quantitative RT-PCR and normalized to GAPDH. The results are represented as fold-induction against the control experiment (empty vector transfection). B and C, total amount of the ER chaperones in HeLa cells transfected with PLP1wt-FLAG and PLP1msd-FLAG. Protein samples from the cells transfected with the indicated vectors were subjected to immunoblotting with the indicated antibodies (B). The amounts of the proteins were measured by densitometry and normalized to β -actin. The results are represented as fold-induction against the control experiment using the empty vector (C). D–F, subcellular fractionation analysis using 0.01% digitonin. Transfected cells were treated with 0.01% digitonin followed by 0.1% SDS, 1% Triton X-100. The extracts of digitonin soluble (left) and insoluble fraction (right) were subjected to immunoblotting with the indicated antibodies (D). The blots were quantitatively analyzed by densitometry to measure the proportion of soluble fraction (E) and insoluble fraction (F) in each protein. Bar graphs are represented as fold-induction \pm S.E. against the mean of control experiment from three independent experiments (*, $p \leq 0.05$; **, $p \leq 0.005$).

Depletion of ER Chaperones and GA Fragmentation in PMD

decreasing their transcription. Furthermore, total protein levels of these chaperones were essentially unchanged in cells transfected with PLP1msd-FLAG (Fig. 2, B and C). These results indicate that PDI, CALR, and GRP78 depletion in the ER is not due to a reduction in the total proteins.

Next, we considered the possibility that PLP1msd affected subcellular localization of the ER chaperones from the ER to another cellular compartment. To test this possibility, transfected cells were treated with 0.01% digitonin, which permeabilizes the plasma membrane but not organelles' membranes, followed by treatment with 0.1% SDS, 1% Triton X-100, which permeabilizes the organelles, including the ER (Fig. 2, D–F). In cells expressing PLP1msd, the proportion of PDI, CALR, and GRP78 in the fraction containing the plasma membrane and cytosol (soluble fraction) was higher than in cells expressing PLP1wt (Fig. 2, D and E). In contrast, the amount of these chaperones was lower in fractions containing the ER (insoluble fraction) in PLP1msd expressing cells (Fig. 2, D and F). Interestingly, the amount of CANX was unchanged in the digitonin-soluble and -insoluble fractions. These results suggest that the decrease in PDI, CALR, and GRP78 in the ER may be due to their translocation from the ER to the plasma membrane or cytosol, but not due to the decrease of total protein.

Recently, Zhang *et al.* (29) reported that ER stress actively promotes GRP78 localization on the cell surface. We confirmed that thapsigargin, a well known ER stressor, increases cell surface expression of PDI in HeLa cells by immunocytochemistry (Fig. 3A) and increases cell surface expression of GRP78 and PDI in HeLa cells by cell surface biotinylation (Fig. 3C). However, we observed no expression of PDI on the cell surface of PLP1msd-transfected cells (Fig. 3B) or no increment of the biotinylated PDI, CALR, and GRP78 in these cells (Fig. 3D). These findings suggest that these mutant proteins induce translocation of the chaperones from the ER to the cytosol, rather to the cell surface.

We speculated that mislocalized cytoplasmic chaperones are degraded through a ubiquitin-dependent ERAD pathway. However, although the amounts of ubiquitinated proteins increased in the presence of proteasome inhibitors, MG-132 or lactacystin (Fig. 3F), those of the ER chaperones were not affected (Fig. 3E), suggesting that they are not degraded through the ERAD pathway after releasing to the cytosol.

Differences and Similarities among Disease-causing Mutations in Other Myelin Genes—To determine whether the depletion of chaperone proteins from the ER is unique to the mutant PLP1 protein or is a common phenomenon observed with mutant proteins encoded by other disease-causing genes, we also examined *PMP22* and *MPZ* genes. Mutations in these genes cause a spectrum of autosomal dominant peripheral demyelinating neuropathies (30).

First, to determine whether accumulation of misfolded proteins in the ER is sufficient to reduce ER chaperone proteins to undetectable levels (by immunostaining) in HeLa cells, we examined two representative *PMP22* mutants, *Trembler-J* (*Tr-J*) (an L16P substitution) and *Trembler* (*Tr*) (a G150D substitution), both of which accumulate in the ER by associating with CANX, however, do not induce UPR (31). Both of *Tr-J* and *Tr* are found in humans (32, 33) and mice (34, 35). First, we

found no increase in the immunoreactivity of CHOP, which is one of the universal markers of ER stress (36), in either *Tr* or *Tr-J*, confirming that these mutants evoked no ER stress (Fig. 4B). We then performed immunocytochemistry with the anti-PDI (Fig. 4, A and C), anti-CALR, and anti-GRP78 (CALR, GRP78, data not shown) antibodies in HeLa cells transfected with the *PMP22*wt or mutant *PMP22* genes. In contrast to our findings in cells transfected with the mutant *PLP1* gene, we observed no depletion of these chaperones from the ER in cells expressing the mutant *PMP22*. These findings indicate that ER accumulation of these mutant proteins, which trigger no ER stress, is insufficient to induce depletion of ER chaperones from the ER.

Next, to analyze whether mutations in another gene that triggers ER stress also deplete the chaperones from the ER, we performed the same experiments using an *MPZ* gene harboring the 506delT mutation (*MPZ506delT*), which induces ER stress and causes a more severe form of peripheral neuropathy, Dejerine-Sottas neuropathy. This frameshift mutation results in 82 residues of shifted amino acid sequence starting from codon 169 in the *MPZ* protein (20). CHOP immunofluorescence was increased in the nucleus of HeLa cells transfected with the *MPZ506delT* gene, but not in cells transfected with the wild-type *MPZ* gene (*MPZwt*) (Fig. 4E), confirming that this mutant protein is an ER stressor. Immunocytochemistry (Fig. 4D) showed that the *MPZ506delT* mutant, but not *MPZwt*, increased the number of cells unstained with anti-PDI antibody (Fig. 4F). These results strongly suggested that depletion of the chaperones from the ER is not induced solely by protein accumulation in the ER, but instead requires both the accumulation of particular mutant proteins and ER stress. In addition, mutations in disease-causing genes other than *PLP1* can elicit the chaperone depletion.

Depletion of PDI, CALR, and GRP78 Is Linked to PMD Severity—Because ER chaperones are connected with protein folding in the ER, we hypothesized that depletion of the ER chaperones may affect the pathogenesis or severity of PMD. We employed two *PLP1* mutants, W163I (11) and I187T (18), both of which result in the mild end of the clinical spectrum of PMD (Fig. 5A). Densitometric analysis of CHOP immunofluorescence in transfected HeLa cells confirmed that these milder *PLP1* mutants activated the UPR, but to a lesser extent than cells transfected with the *PLP1msd* gene (Fig. 5B).

Next, to analyze whether ER chaperone depletion is associated with clinical severity, we compared the expression of PDI in HeLa cells transfected with these *PLP1* mutant genes. We found that the proportion of PDI-unstained cells expressing FLAG-tagged *PLP1-W163L* or *PLP1-I187T* was significantly lower than that of cells expressing *PLP1msd* (Fig. 5C). In addition, we observed a similar tendency in cells expressing the *MPZ* mutants. A mild *MPZ* allele, *MPZS63del*, evoked less ER stress and resulted in a smaller proportion of “PDI-unstained cells” than a severe allele, *MPZ506delT* (data not shown). Together, these results strongly suggest a potential linkage between chaperone depletion and the phenotypic variation in ER stress-related disorders.

Depletion of ER Chaperones and GA Fragmentation in PMD

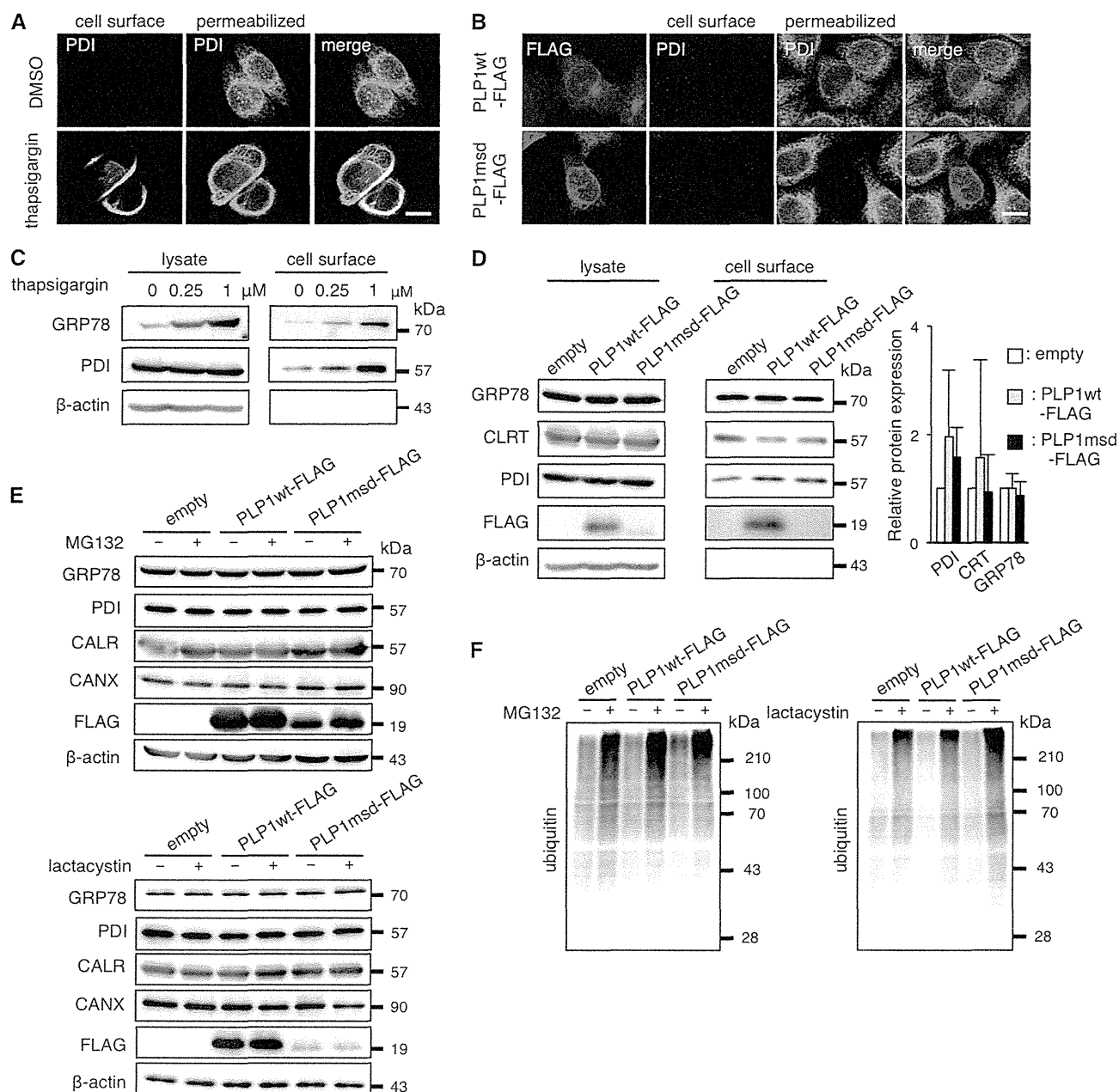


FIGURE 3. PLP1msd does not increase cell surface expression of the ER chaperones. *A* and *B*, immunocytochemical analysis of cell surface PDI on HeLa cells treated with 1 μM thapsigargin (*A*) or transfected with the PLP1msd gene (*B*). Cell surface PDI (green) were stained with the anti-PDI antibody without permeabilization followed by intracellular staining with the same antibody (magenta). Scale bar, 10 μm. *C* and *D*, biochemical analysis of cell surface expression of the ER chaperones. HeLa cells were treated with thapsigargin for 16 h (*C*). Transfection was performed before 24 h of cell surface biotinylation (*D*). Cell surface proteins were labeled with biotin, precipitated with streptavidin beads followed by immunoblotting with anti-PDI, anti-CALR, and anti-GRP78 antibodies. *E* and *F*, protease inhibitors do not increase total amounts of the ER chaperones in HeLa cells expressing PLP1msd. Transfected cells were treated with 5 μM MG132 for 16 h or 1 μM lactacystin for 8 h followed by immunoblotting with the anti-PDI, anti-CALR, anti-GRP78, anti-CANX (*E*) and anti-ubiquitin antibodies (*F*). Protein amounts were measured by densitometry. The results are represented as fold-induction against the control experiment using the empty vector. Values are represented as the mean ± S.E. from three independent experiments (*D*).

AQ:D

Down-regulation of Pdi in the SC and Primary Culture of *msd* Mice—In our *in vitro* analyses, expression of the PDI, CALR, and GRP78 proteins did not increase in cells expressing PLP1msd, despite the significant increase in their transcripts (Fig. 2*A*). To determine whether this also occurs *in vivo*, we further investigated the mRNA and protein expression of these ER chaperones in the SCs isolated from male *msd* mice, which

carry the *Plp1A243V* allele, on P14, when the *Plp1* gene is most strongly expressed in the SCs of mutant mice (8). Expression of the *Chop* transcript was significantly higher in *msd* mice than in wild-type mice, suggesting that cells in the SCs of *msd* mice were under ER stress (Fig. 6*A*). We then analyzed the expression of these ER chaperone mRNA by quantitative RT-PCR (Fig. 6*B*). The expression of *Grp78* mRNA was significantly

F6

Depletion of ER Chaperones and GA Fragmentation in PMD

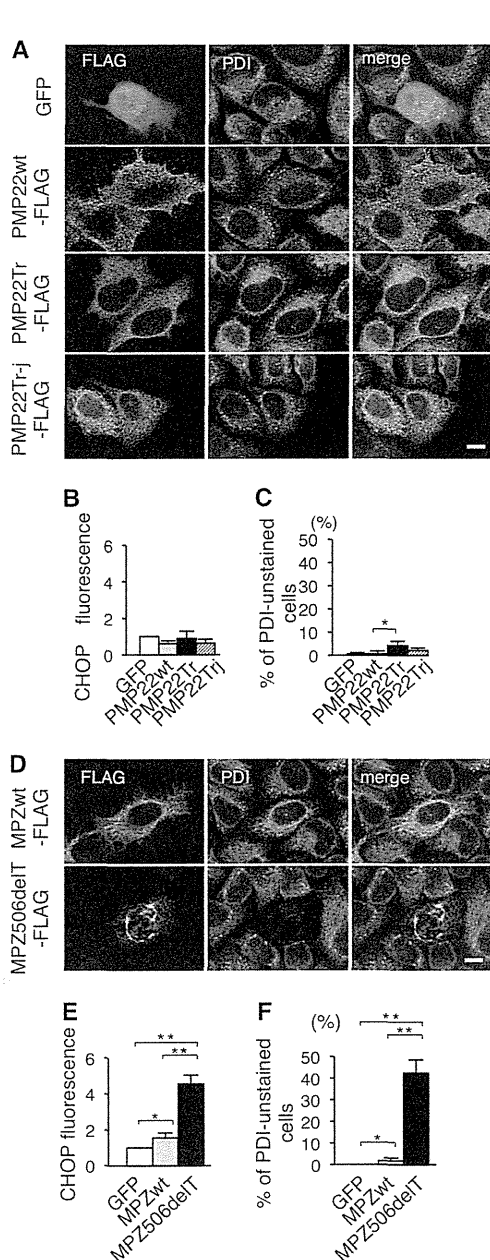


FIGURE 4. Effect of PMP22 and MPZ mutations on ER chaperones. A and D, immunocytochemistry of PDI in HeLa cells transfected with the PMP22wt and mutant PMP22 genes (A) or the MPZwt and MPZ506delT genes (D). HeLa cells transfected with the indicated vectors were immunostained with the anti-FLAG (green) and anti-PDI (magenta) antibodies followed by observation with a confocal fluorescence microscope. Note that cells expressing MPZ506delT showed an extremely faint staining pattern for PDI (arrowhead). Scale bar, 10 μ m. B and E, relative expression of CHOP in HeLa cells transfected with the PMP22wt and mutant PMP22 genes (B) or the MPZwt and MPZ506delT genes (E). HeLa cells transfected with the indicated vectors were stained with the anti-FLAG and anti-CHOP antibodies together with DAPI to visualize the nuclei. The relative fluorescence intensity of CHOP in the nuclei was analyzed by densitometry. C and F, proportion of unstained cells with anti-PDI antibody in HeLa cells transfected with the PMP22wt and mutant PMP22 genes (C) or the MPZwt and MPZ506delT genes (F). Bar graphs are represented as fold-induction \pm S.E. against the mean of control experiment from three independent experiments with >100 cells counted in each experiment (*, $p \leq 0.05$; **, $p \leq 0.005$).

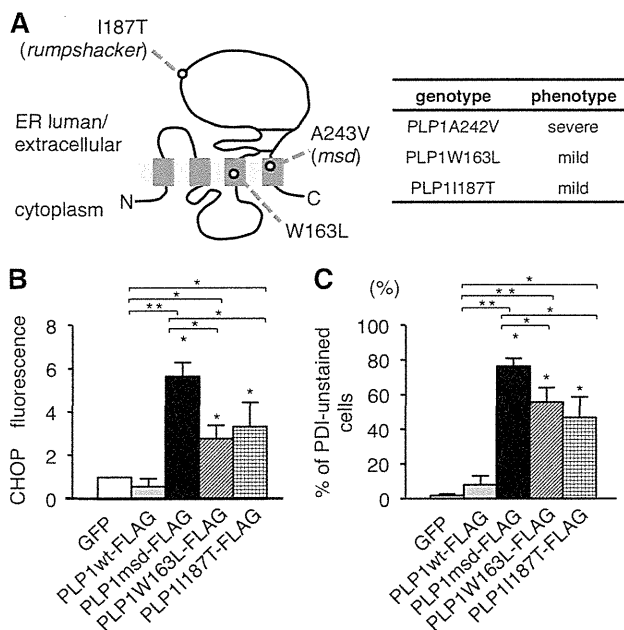


FIGURE 5. Effect of different PLP1 mutations on ER chaperones. A, schematic diagram of PLP1 with the positions of mutations examined in this study (left) and their associated phenotypes (right). B, expression of CHOP in HeLa cells transfected with the PLP1wt and mutant PLP1 genes. The fluorescence intensity of CHOP in the nuclei was analyzed by densitometry as described in the legend to Fig. 4B. C, proportion of unstained cells with anti-PDI antibody in HeLa cells transfected with PLP1wt and the indicated PLP1 mutant genes as described in the legend to Fig. 4C. Bar graphs are represented as fold-induction \pm S.E. against the mean of control experiment from three independent experiments with >100 cells counted in each experiment (*, $p \leq 0.05$; **, $p \leq 0.005$).

increased (2-fold) in *msd* mice. *Pdi* and *Calr* were also up-regulated, but to a lesser extent. However, at protein levels, we observed discordance (Fig. 6, C and D). *Pdi* protein expression in *msd* mice was significantly decreased. The expression of *Calr* showed a similar tendency, although these results did not reach significance ($p = 0.06$). In contrast, *Grp78* and *Canx* protein expression did not differ significantly when compared with wild-type mice.

We also immunocytochemically examined primary MGCs isolated from the brains of embryonic day (E) 14.5 wild-type or *msd* mice. On the 4th day after induction of oligodendrocyte differentiation, profound maturation with increased MBP immunoreactivity was evident in the wild-type MGCs (Fig. 6E). In contrast, rapid regression of Oligo2-positive cells and decreased MBP immunoreactivity were observed in the *msd* MGCs, suggesting that oligodendrocyte maturation induced apoptosis in *msd* on the 4th day after induction. *Pdi* was detected in the cell body of *Plp1*-positive mature oligodendrocytes in wild-type MGCs, whereas, it was only faintly stained in *Plp1*-positive oligodendrocytes in the *msd* MGCs. (Fig. 6F). These results suggest that endogenous PLP1*msd* depletes *Pdi* from the ER of the oligodendrocytes.

Inhibition of GA to ER Transport Is Associated with the Disappearance of PDI, CALR, and GRP78—To determine the underlying mechanism for PDI, CALR, and GRP78 depletion from the ER in cells expressing PLP1 mutants, we further analyzed the effects of the following chemical ER stressors on the

Depletion of ER Chaperones and GA Fragmentation in PMD

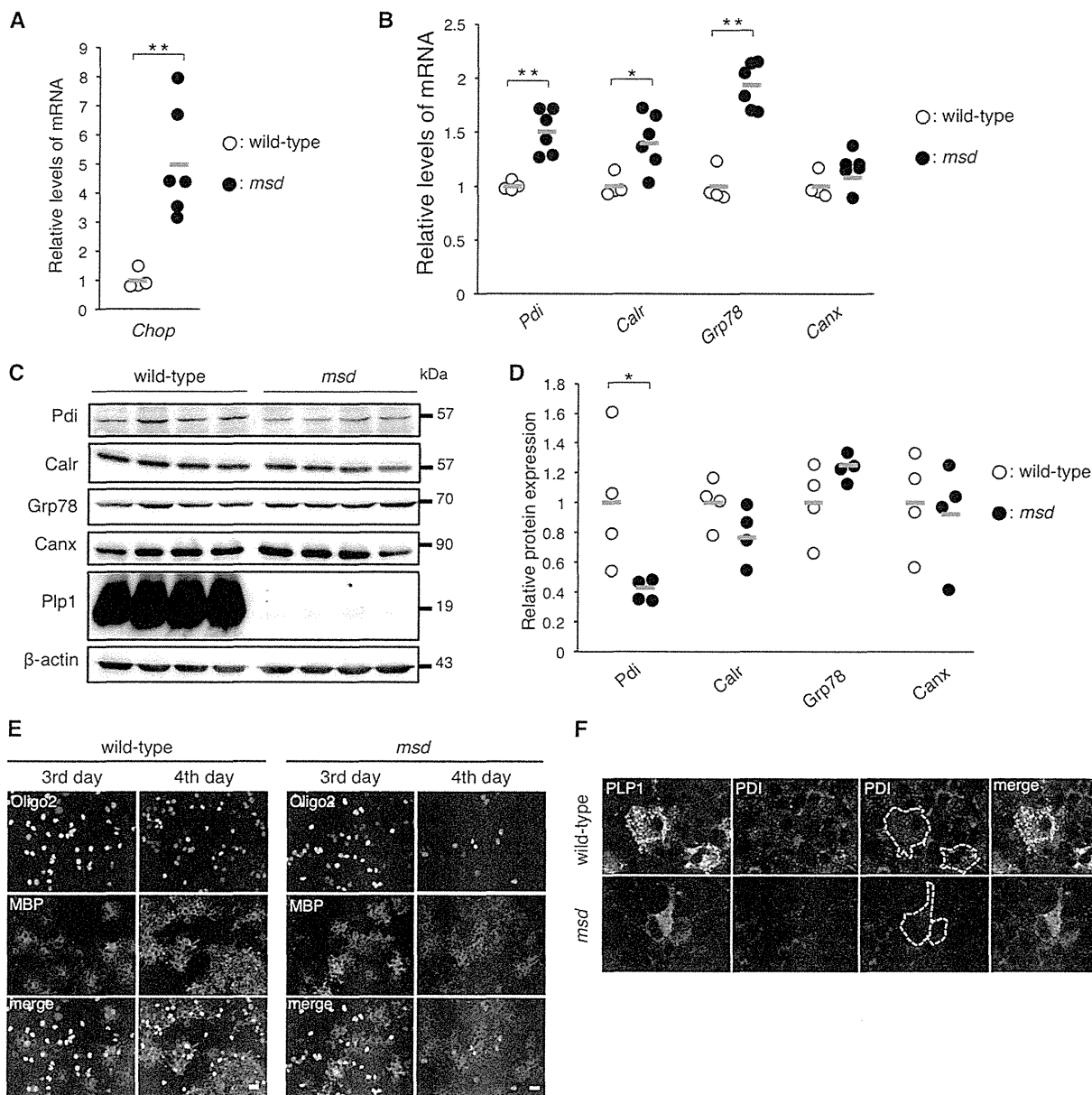


FIGURE 6. PDI is down-regulated in the SCs and primary oligodendrocytes of *msd* mice. *A* and *B*, quantitative analysis of *Chop* (*A*), *Pdi*, *Calr*, *Grp78*, and *Canx* genes (*B*) in the SCs of *msd* mice. Quantitative RT-PCR was performed to analyze the expression levels of *Pdi*, *Calr*, *Grp78*, and *Canx* in the SCs of wild-type (open circle, *n* = 4) and *msd* (filled circle, *n* = 6) mice at P14. *GAPDH* was used as an internal control. The results are represented as fold-induction against the means of wild-type mice. Red horizontal bars indicate the mean. *C* and *D*, relative amounts of ER chaperones in the SCs of *msd* mice. The SCs of P14 wild-type (open circle, *n* = 4) and *msd* (filled circle, *n* = 4) mice were subjected to immunoblotting with the indicated antibodies (*C*). The amounts of the proteins were measured by densitometry and normalized to β -actin (*D*). *E*, expression of MBP and Oligo2 in primary oligodendrocytes from *msd* mice. Immunocytochemistry of MBP and Oligo2 in primary oligodendrocytes of *msd* mice. Primary mixed glial cultures were prepared from the forebrains of E14.5 wild-type or *msd* mice. On the 3rd and 4th days after induction of oligodendrocyte differentiation, the oligodendrocytes were immunostained with anti-MBP (magenta) and anti-Oligo2 (green) antibodies and observed with a confocal fluorescence microscope. Scale bar, 5 μ m. *F*, immunocytochemistry of PDI in primary oligodendrocytes of *msd* mice. Primary oligodendrocytes prepared from the forebrains of wild-type or *msd* mice at E14.5 and immunostained with anti-PLP1 (green) and anti-PDI (magenta) antibodies and observed with a confocal microscope. Scale bar, 5 μ m. *A*, *B*, and *D*, *, *p* \leq 0.05; **, *p* \leq 0.005.

expression of ER chaperones: thapsigargin, a sarco/endoplasmic reticulum Ca^{2+} -ATPase inhibitor; tunicamycin, an *N*-glycosylation inhibitor, and brefeldin A (BFA), a GA-ER transport inhibitor. These three compounds greatly up-regulated the transcripts of *CHOP* and *GRP78*, confirming that they work as ER stressors (Figs. 7, *B* and *C*, and 8, *B*, *C*, *E*, and *F*). These compounds also slightly but significantly increased the expression of *PDI*, *CALR*, and *CANX* transcripts.

Next, HeLa cells were treated with these compounds for 8 h, followed by immunocytochemistry with anti-PDI, anti-CALR, anti-GRP78, or anti-CANX antibodies. Thapsigargin and tunicamycin did not alter the expression of the chaperones (Fig. 8*A*), even after an extended incubation (Fig. 8*D*). In contrast, BFA treatment clearly diminished PDI, CALR, and GRP78 from the ER; however, CANX expression remained unchanged (Fig. 7*A*). In BFA-treated HeLa cells, total amounts of the chaperone

F7,8